Of Patches, Predators and Policies: Mathematical Stories from Land and Sea

By

Appilineni Kushal
DISSERTATION

Submitted in partial satisfaction of the requirements for the degree of

DOCTOR OF PHILOSOPHY

in

APPLIED MATHEMATICS

in the

OFFICE OF GRADUATE STUDIES

of the

UNIVERSITY OF CALIFORNIA

DAVIS

Approved:

Alan Hastings, Chair

Fernanda S Valdovinos

Michael Springborn

Committee in Charge

2025

To my parents — it all starts with your blessings
To the voice inside my head — we did it *again*

Contents

Abstract v

Acknowledgments vi

Introduction 1

Chapter 1. Effect of Migrations on Synchrony in Host-Parasitoid system 4

Abstract 4

1.1. Introduction 4

1.2. Single patch dynamics 7

1.3. Two patch dynamics 9

1.4. Robustness across choice of functions 13

1.5. Length of the cycle 15

1.6. Cellular Automata model 19

1.7. Discussion and Conclusion 22

Chapter 2. Effect of Spatial Heterogeneity in Spatial Metapopulation models 26

Abstract 26

2.1. Introduction 27

2.2. Host-Parasitoid dynamics in Single and Two-Patch Systems 28

2.3. Spatially explicit metapopulation model 30

2.4. Results 34

2.5. Discussion 39

2.6. Code availability 43

2.7. Acknowledgements 43

Chapter 3. Assessing Impacts of Bycatch Policies and Fishers' Heterogeneous Information on Food Webs and Fishery Sustainability 44

Abstract 44
3.1. Introduction 44
3.2. Methods 47
3.3. Results 54
3.4. Discussion 58
Code availability 60
Funding 60
Acknowledgements 60
Conclusion 61
Appendix A. Supplementary to Chapter 1 and 2 62
Supplementary Information 62
Bibliography 64

Abstract

Ecological systems are shaped by nonlinear interactions, spatial structure, and, increasingly, human interventions. Understanding the mechanisms that drive species persistence, oscillations, and spatial pattern formation is essential for predicting ecological outcomes and designing effective management strategies. This dissertation uses a suite of mathematical models—including discrete-time and continuous-time dynamical systems, spatially explicit metapopulations, and ecological networks—to explore the dynamics of insect herbivores, their parasitoid enemies, and multispecies fisheries systems.

The first part of this work focuses on host-parasitoid dynamics across habitat patches. Using discrete-time models, we show how migration influences the synchrony of population outbreaks, identifying parameter regimes that support in-phase or out-of-phase oscillations. These results are shown to be robust across a variety of functional forms for parasitism and competition. Extending this analysis to larger, heterogeneous landscapes, we explore how even modest habitat loss can disrupt spatial synchrony, reduce population densities, and generate novel spatial phenomena such as spiral waves—emerging from the interplay between local dynamics and spatial heterogeneity.

In the final part of the dissertation, we develop a continuous-time ecological network model of fisheries that incorporates both species interactions and heterogeneous human harvesters. We examine how bioeconomic feedbacks and quota-based management policies affect ecological resilience and economic outcomes. By simulating multiple food webs and policy scenarios, we highlight trade-offs between conservation, profit, and harvest sustainability.

Together, these studies demonstrate the power of mathematical modeling in revealing general principles of ecological dynamics and informing management strategies in complex, coupled human-natural systems.

Acknowledgments

As the saying goes, "*It takes a village to raise a child.*" While I am no longer a child, this PhD journey has reminded me of how deeply true that sentiment remains. My Indian heritage has always emphasized the role of community in shaping individual success. This achievement is no exception—I owe it to the many people who supported me throughout my time in graduate school.

I begin by thanking my parents, who have always encouraged me to carve my own path, even when it diverged from tradition. Their emotional support and sacrifices made this PhD possible. My father sparked my love for mathematics early on; some of my fondest childhood memories are of working on Math and Physics Olympiad problems together. Those long conversations laid the foundation for my academic path.

I'm grateful to my extended family, especially my cousin Appilineni Disanth, for shielding me from the challenges back home and taking care of my family's needs during the global pandemic. His support allowed me to focus on my research with clarity and single-minded determination.

I am deeply thankful to Alan Hastings for the opportunity to be his student and for his mentorship over the past six years. As an undergraduate, I had read his work, and it felt surreal to be accepted into a PhD program where I could work with him. I still remember the night I received my offer—I couldn't sleep, knowing how life-changing it would be. Six years later, I know that it truly was.

I would also like to thank Fernanda Valdovinos for welcoming me into her lab, even though I already had an advisor. She believed in my ability to manage independent projects and supported me as I stepped into a new research area on fisheries. Her guidance and encouragement were instrumental in helping me pursue interdisciplinary work. I was thrilled when she joined UC Davis, having earlier expressed my interest in working with her while she was at Michigan. I also want to extend my sincere thanks to Michael Springborn for mentoring me through the fisheries project, offering valuable feedback, and letting me develop my own questions at the intersection of ecology and economics—despite my lack of formal background in either. I'd also like to thank other faculty members at UC Davis with whom I've had fruitful discussions—Sebastian Schreiber, Tim Lewis,

and Marissa Baskett, to name a few.

I am grateful to my labmates in Fernanda's group— Taran, Sophia, Sabine, Casey, Kayla, Marco, Lauren, Alaina and Rebecca—for their camaraderie, support, and technical help. Coming to work was genuinely fun because of them. I also thank Tina Denena from the Department of Mathematics and Statistics and Jennifer Carriere from Environmental Science and Policy for helping me navigate many logistical hurdles.

I'd be remiss not to mention those outside academia who stood by me. I'm especially grateful to my therapist, Blanca, for helping me navigate the mental health hurdles I've battled for a long time. Thank you to Becca, Emily, and Melanie for their unwavering emotional support during the highs and lows of the past two years. To my friends in Davis and Sacramento—Sudheer, Shriya, Lauren, Shisham, Girish, Xue, Davi, Jorge—thank you for making this place feel like home. I'm also grateful to my friends from back home — Chinmay, Agniva, Shubham, Anurag, Yogesh, Anshuman, Tara and Sabyasachi for the conversations, travel, and shared experience of navigating grad school. And to my teammates from Microbes—Eduardo, Courtney, Tyler, Hadi, Dino, Pedro, Maritza, Ben, to name a few—thank you for helping me pursue my love of football (soccer) while juggling academic life (no pun intended).

I've always found deep inspiration in sports. The discipline, hard work, persistence, and humility that define athletic excellence have mirrored my own academic journey. As a lifelong football fan, watching Lionel Messi win the World Cup in 2022 was a profoundly emotional moment. His journey to win something with his national team—from near misses in 2007, 2014, 2015 and 2016 to ultimate triumph in 2022—reminded me that perseverance through setbacks can lead to extraordinary outcomes. That story became a wellspring of hope through the hardest stretches of my PhD. GOAT, for a reason.

Introduction

Mathematical modeling and simulation have become cornerstone tools in developing ecological theory, providing a quantitative framework to analyze complex biological systems. These tools allow us to uncover the fundamental governing principles of ecological systems and make predictions by combining biological insight with tractable models. Ecological systems are complex, nonlinear, and often spatially structured, with interactions across multiple spatial and temporal scales—conditions where intuition alone is insufficient for accurate prediction. Through the construction and analysis of mathematical models, it becomes possible to dissect key mechanisms, explore parameter regimes, and uncover general principles that govern ecological persistence, oscillations, and stability. From understanding outbreak cycles in insect populations to predicting the effects of fisheries management on marine ecosystems, such models serve as a bridge between ecological questions and quantitative predictions.

This dissertation lies at the intersection of applied mathematics and theoretical ecology, using discrete-time and continuous-time models, spatially implicit and explicit frameworks, and ecological network theory to investigate how movement, spatial structure, species interactions, and human interventions shape ecological dynamics. Across diverse biological systems—from host-parasitoid interactions to fisheries dynamics—a common goal is to develop models that are simple enough to yield analytical and computational insights, yet detailed enough to capture essential ecological processes. Although the systems studied differ in biological details, they share common challenges: understanding persistence, oscillations, species interactions, and the consequences of heterogeneities and human interventions in the form of biological control or management policies. Through a combination of mathematical analysis and numerical simulation, this work advances our understanding of ecological systems under both natural and anthropogenic pressures.

The first part of this work examines the role of dispersal in synchronizing simple discrete-time host-parasitoid models. In ecological systems where local populations are coupled by movement, dispersal can synchronize or desynchronize oscillations, alter extinction risks, and generate complex

spatial patterns. To investigate this, classical models of host-parasitoid dynamics, often studied in isolated patches, are extended to a two-patch framework where movement between patches induces novel dynamical behaviors. Using a combination of linear stability analysis, bifurcation theory, and numerical simulations, we investigate how migration between habitat patches influences outbreak dynamics, with particular focus on conditions under which oscillations in neighboring patches become synchronized or remain out of phase. Moving beyond specific functional forms, we emphasize the robustness of these patterns across alternative biological assumptions. We further extend the analysis to biologically independent cellular automata models, highlighting how general mirgation and update rules create the same synchronized outcomes as that of a biological model.

Building on these results, the second part extends the two-patch model into a metapopulation framework and introduces spatial heterogeneity. Natural landscapes are rarely homogeneous; habitat loss, fragmentation, and barriers to dispersal are ubiquitous. By modeling habitat as a lattice of discrete patches, with a fraction rendered uninhabitable, we investigate how small-scale heterogeneities affect population persistence and spatial synchrony. Two alternative dispersal rules—absorbing and reflecting at the boundary of uninhabitable patches—are considered to disentangle structural effects from demographic mortality during movement. Incorporating spatial heterogeneity into host-parasitoid models reveals that even small amounts of habitat loss can disrupt spatial synchrony and alter mean population densities, with effects that depend critically on behavioral assumptions about movement near uninhabitable patches. We also highlight new causes for the emergence of widely studied spiral wave patterns, thus underscoring the importance of considering spatial structure explicitly when extrapolating theoretical predictions to real-world systems.

The final part of the dissertation shifts to continuous-time ecological network models to study the interplay between ecological interactions, human harvesting, and management policies. Fisheries provide an ideal system to examine the tension between ecological sustainability and economic incentives. Traditional fisheries models often neglect species interactions, focusing on single-species dynamics. Moving beyond these, we employ an allometric trophic network (ATN) framework, based on ordinary differential equations parameterized by metabolic scaling laws, to capture species interactions within marine food webs. Human harvesters, modeled as additional dynamic nodes

connected to target and bycatch species, introduce bioeconomic feedbacks into the network. Heterogeneity among fishers—reflecting differences in catch efficiency and bycatch avoidance—is incorporated to reflect realistic variation in fishing strategies. This framework allows us to evaluate how different management policies, such as quota-based closures, affect both ecological outcomes (species persistence, biodiversity) and economic outcomes (profitability, season length). Through this bioeconomic model, we evaluate trade-offs and identify strategies that promote long-term sustainability.

Across all chapters, a unifying methodological approach is emphasized: the construction of minimal models that retain essential biological realism while allowing for analytical tractability and systematic exploration of parameter space. Numerical simulations complement analytical work where necessary, particularly in regimes characterized by complex dynamics such as chaos or emergent spatial patterns. While acknowledging the inevitable trade-offs between model simplicity and ecological realism, this work aims to identify mechanisms that persist across model structures, functional forms, and ecological contexts. In sum, this dissertation contributes to the broader goals of theoretical ecology and applied mathematics by developing, analyzing, and interpreting mathematical models that reveal how ecological systems respond to spatial structure, movement, interaction networks, and human interventions.

CHAPTER 1

Effect of Migrations on Synchrony in Host-Parasitoid system

Abstract

Insect outbreaks can cause large scale defoliation of forest trees or destruction of crops, leading to ecosystem degradation and economic losses. Some outbreaks occur simultaneously across large geographic scales and some outbreaks occur periodically every few years across space. Parasitoids are a natural enemy of these defoliators and could help mitigate these pest outbreaks. A holistic understanding of the host-parasitoid interactions in a spatial context would thus enhance our ability to understand, predict and prevent these outbreaks. We use a discrete time deterministic model of the host parasitoid system with populations migrating between 2 patches to elucidate features of spatial host outbreaks. We show that whenever populations persist indefinitely, host outbreaks in both patches can occur alternatively (out of phase) at low migration between patches whereas host outbreaks always occur simultaneously (in phase) in both patches at high migration between patches. We show that our results are robust across a large range of parameters across different modelling approaches used typically to model intraspecific competition among hosts and parasitism, in the host-parasitoid literature. We give an analytical expression for the period of oscillations when the migration is low i.e., when host outbreaks in both patches are out of phase, show it is in agreement with numerical results. We end our paper by showing that we get the same results whether we include the biologically rooted formulations from [92] or a general cellular automata model with qualitative rules.

1.1. Introduction

It is long known that insect herbivores are agents causing threats to ecosystems - threatening irreversible changes to food security, forest cover, etc. [11], [22], [44]. These insect populations can remain at a low density for many years, often going unnoticed. However, every few years, these insect populations explode in numbers, causing large scale loss of forest cover [86], [73]. Classical biological control is a way to deal with these outbreaks, where a foreign species (natural enemy) is

purposefully introduced and established to suppress the outbreaks of the native species [23], [29]. Pests which can be controlled by introducing natural enemy includes invertebrates, vertebrates and weeds. The organisms that function as natural enemy include vertebrates (birds, reptiles) and invertebrates (parasitoids). Here, we focus our attention on herbivore insect populations and the parasitoids which attack them.

Parasitoids have long been a subject of ecological interest for several reasons. Roughly 14% of all insect species are parasitoids [57]. The female parasitoid searches for an immature stage of the herbivore insect (host) and lays eggs inside it. These eggs hatch inside the body of the host and the parasitoid larvae feed and grow at the expense of hosts, inside the host. At a later stage, they emerge from the host, typically killing it in the process. Thus, parasitoids are considered agents of biological control as they can keep the herbivore insect populations to low numbers by direct mortality [125], [128], [48], [115].

There are several simplifications which make the study of host-parasitoid system more suited to study enemy-victim dynamics than more general predator prey dynamics. Many parasitoids are highly specific to the hosts they predate [115], allowing us to consider the host-parasitoid system as a closed system, independent of the influence of other populations. Furthermore, this specificity also leads to synchronized life cycles of host and parasitoid species, allowing the use of discrete time equations appropriate. Since hosts are attacked only by adult parasitoids, we can further ignore age structure in our modelling [94].

Population oscillations are an important characteristic of many outbreaking foliage eating insects dynamics and this is often related to large scale spatial synchrony [78]. There has been many theoretical studies understanding these oscillations [121], [2], pinning these oscillations to parasitism, food limitation etc., without considering the spatial extent of these processes and hence missing the full picture of spatial synchrony. For insect outbreaks, which often have large amplitude oscillations, previous works have suggested the effect of migration to be a key driver [49]. Migration is of crucial importance in unraveling the dynamics of spatial synchrony in insect populations [3], [87].

Migration can introduce traveling population waves, leading to complex relationships between synchrony and distance [87], [58]. Migratory movements can synchronize the dynamics of different species, including those with direct trophic interactions and shared resources [87]. Investigating migration patterns can lead to insights into the mechanisms driving spatial synchrony which is vital for predicting and managing insect outbreaks, understanding ecological interactions, and effectively conserving and controlling insect populations.

Spatial synchrony has long been studied in ecology, both in host-parasitoid systems [4], [58] and more generally predator-prey models [75], [60], [49], in both continuous and discrete time framework. Despite the rich literature, the relationships between regulatory factors (such as intraspecific competition, parasitism etc.), migration and spatial synchrony still remains elusive due to lack of consensus. One reason for the lack of consensus is the strong assumptions and specificity of the modelling frameworks used, as dynamical systems (and the emergent behavior) are sensitive to the choice of modelling frameworks involved. Furthermore, focus is often on the stabilizing or destabilizing effects of migration [3], [75], [107] on the persistence of oscillations, with emphasis on stability and bifurcation analysis. This misses important features of the coupled spatial system like frequency of oscillations, which is difficult to infer from bifurcation diagrams especially if the underlying dynamics are chaotic and the resulting oscillations are out of phase. Out of phase oscillations are stable as the populations are less prone to local extinction due to recolonization from adjacent patches [24]. Out of phase oscillations have been shown in empirical studies [96], [123] and numerical studies [58], [4]. But analytical insights into them are limited to continuous time models where theory of weakly coupled oscillators is useful [49], [126] or simple discrete models [59], [51] with period 2 cycles.

We aim to fill some of these gaps in our study using a discrete time host-parasitoid system in 2 patches, with migration between them. Given the rather strong assumptions made in most spatial host-parasitoid models, it could appear that drawing conclusions about a specific biological system could be difficult. We address this gap here by trying to demonstrate robust results that should apply across a range of systems. For example, in Section 3, we show that at low migration, the host outbreaks in the 2 patches occur alternatively (out of phase) and at high migration, the host

outbreaks in both patches occur simultaneously (in phase). While similar results for host-parasitoid systems have been shown before [4], we focus our attention to the robustness and cause of such oscillations, which is novel. We address the robustness (in Section 4) by testing our results across different biologically relevant functional forms for intraspecific competition and parasitism. Later in Section 6, we also show that similar results are obtained in a cellular automata model devoid of biological detail, which only qualitatively captures host-paraisioid systems, thus establishing the role of migration independent of other biological interactions. Furthermore, we provide an analytical expression for the time period of oscillations, when patches oscillate out of phase, something that is often limited to simpler discrete time models. We show a comparison of our analytical results with numerically obtained time period in Section 5.

1.2. Single patch dynamics

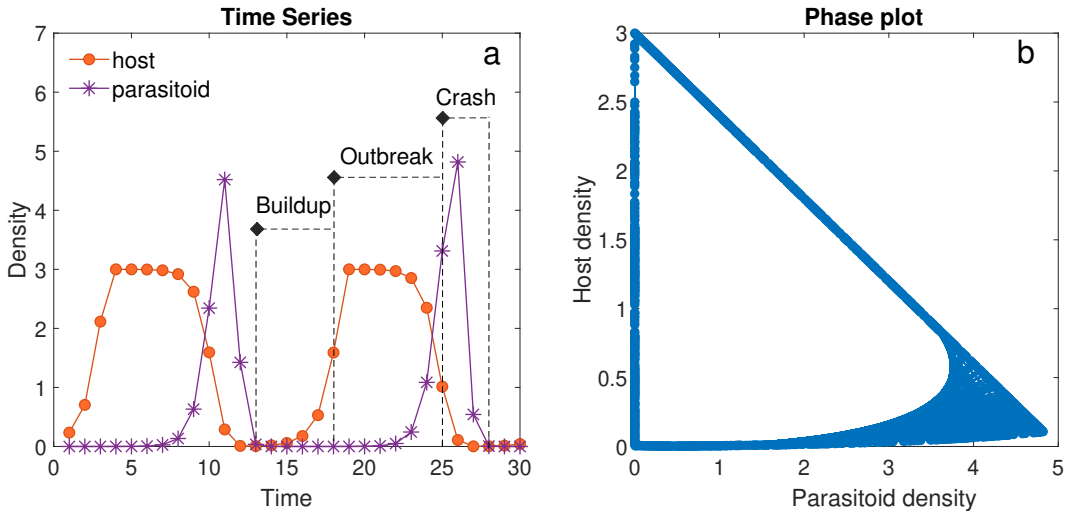

FIGURE 1.1. a) Time series and b) phase plot of a single host-parasitoid population at steady state is shown. The 3 stages i.e., Buildup, Outbreak and Crash is shown, with the diamond on the left showing the included generation in each stage. As shown, the densities show a quasi-periodicity, where they are confined within a manifold as shown in (b).

We use the general formulations from [92], which models 3 phenological processes - reproduction, intraspecific competition amongst hosts and parasitism (by parasitoids). This gives a general form for annual densities for hosts (H_t) and parasitoids (P_t)

$$H_{t+1} = \lambda F(H_t) G(H_t, P_t)$$

$$P_{t+1} = cF(H_t)(1 - G(H_t, P_t)) \tag{1.1}$$

Here λ is the intrinsic growth rate of the hosts and c is the number of parasitoids that emerge from a single larva. Following the analysis done in [121], we assume the following form of non-dimensionalized equations for the host-parasitoid dynamics within each patch, where the min function is used to model intraspecific competition. It is exactly compensatory, as opposed to Ricker or many other forms of intraspecific competition which are over compensatory. This model has an unstable fixed point and thus leads to oscillations as shown in Figure 1.1.

$$h_{t+1} = \lambda \min(h_t, 1) e^{-p_t}$$

$$p_{t+1} = \gamma \min(h_t, 1)(1 - e^{-p_t}) \tag{1.2}$$

The oscillations produced by this model (as shown in Figure 1.1 a) can be roughly divided into 3 stages i.e., 1) Buildup - which is marked by low host and parasitoid densities i.e., $1 > h_t$ (typically $h_t \approx 0$ for all but the last generation of buildup) and $p_t \approx 0$ (see Supplementary Figure 1). During buildup, the effect of intraspecific competition and parasitism on host densities are negligible, thus Equation 2 for host reduces to $h_{t+1} \approx \lambda h_t$, leading to geometric growth. This is followed by 2) Outbreak - which is marked by high host density but low parasitoid density i.e., $h_t \approx \lambda > 1, \ln \lambda > p_t$ (typically $p_t \approx 0$ for all but the last generation of outbreak) (see Supplementary Figure 1). Intraspecific competition amongst hosts reduces host densities every generation, but the mortality due to parasitism is still negligible. Thus, the host densities remain high post reproduction every generation. Because hosts are abundant, parasitoids grow geometrically during outbreaks as Equation 2 reduces to $p_{t+1} = \gamma(1 - e^{-p_t}) \approx \gamma p_t$. Outbreak is followed by 3) Crash - where the parasitoid population is large enough to reduce host population significantly (i.e., $p_t > \ln \lambda$). Typically, crash lasts for 2-3 generations, as shown in Figure 1.1 a.

1.3. Two patch dynamics

Let h_t^i, p_t^i be the host and parasitoid population in patch i at time t. Let λ be the growth rate of the host and γ be the growth rate of parasitoid. Let ϵ be the fraction of population migrating from one patch to another. The equations for the resulting dynamical system is:

$$
\begin{aligned}
h_{t+1}^1 &= h_{tm}^1(1-\epsilon) + \epsilon\, h_{tm}^2 \\
h_{t+1}^2 &= h_{tm}^2(1-\epsilon) + \epsilon\, h_{tm}^1 \\
p_{t+1}^1 &= p_{tm}^1(1-\epsilon) + \epsilon\, p_{tm}^2 \\
p_{t+1}^2 &= p_{tm}^2(1-\epsilon) + \epsilon\, p_{tm}^1
\end{aligned} \tag{1.3}
$$

Here h_{tm}^i, p_{tm}^i represent the host and parasitoid densities in patch i at t before migration after competition, parasitism and reproduction have taken place i.e.,

$$h_{tm}^i = \lambda \min(h_t^i, 1) e^{-p_t^i} \tag{1.4}$$

$$p_{tm}^i = \gamma \min(h_t^i, 1)(1 - e^{-p_t^i}) \tag{1.5}$$

In our model, reproduction is given by a multiplicative factor, thus, the order of migration and reproduction can be interchanged. Biologically, it'll refer to the scenario where the surviving adults after competition and parasitism have taken place, migrate and then reproduce.

When $\epsilon \to 0$, both patches oscillate almost independently i.e., the effect of coupling due to migration between patches is negligible. Note that the parameters are identical in both the patches.

As we increase the strength of coupling due to migration i.e., ϵ from 0, we first get out of phase solutions (as shown in Figure 1.2 (b)), where the peaks in host densities (i.e., host outbreaks) in 2 patches occur alternatively (out of phase). These out of phase oscillations persist indefinitely in our simulations as long as the initial conditions in the 2 patches aren't very identical. If the initial conditions are identical, then both patches behave as one single patch and thus, they oscillate in unison. In our simulations, initial conditions were selected randomly and the host densities of 2

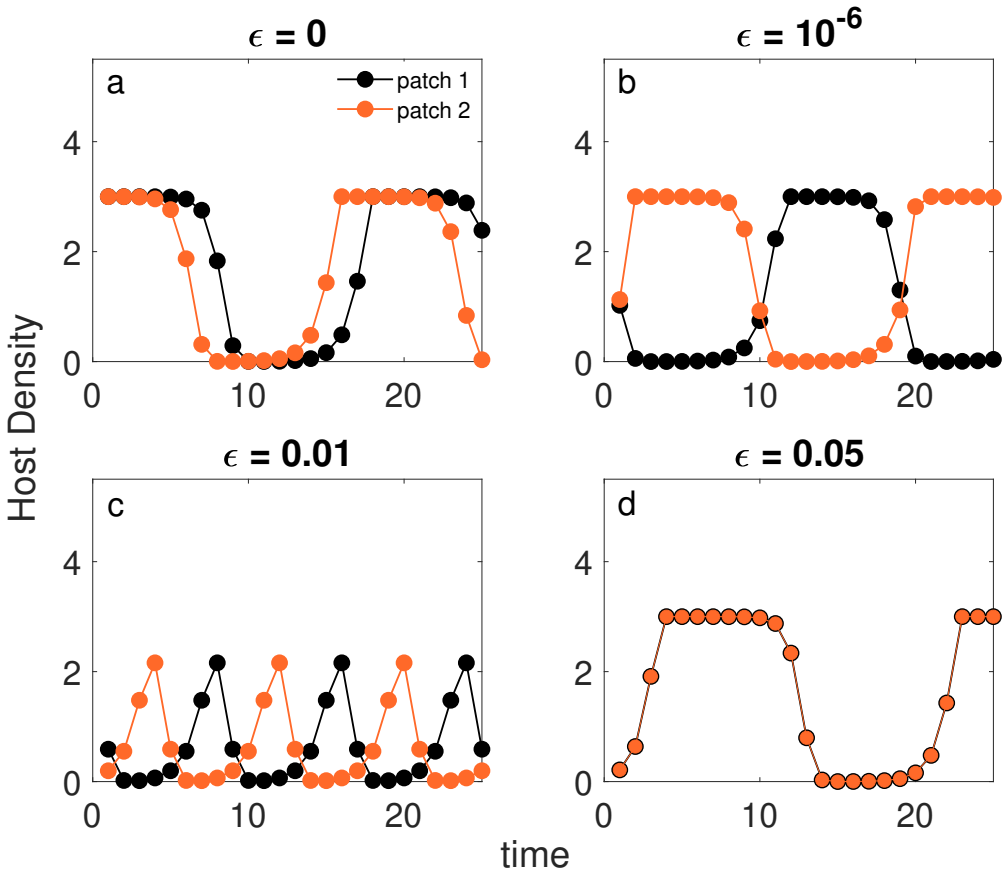

FIGURE 1.2. Host densities at steady state are shown for different migration rates. The parameters $\lambda = 3$, $\gamma = 6$ were fixed. In (a), there is no coupling between the patches. However, when we increase ϵ, we see out of phase solutions (b, c), where the host outbreaks in the 2 patches occur alternatively. These out of phase solutions exist for a large range of ϵ values. Increasing ϵ, the time period of host outbreaks decrease till the outbreak occurs for 1-2 generations (as shown in (c)). With further increase in migration, the host outbreaks in both the patches occur simultaneously as shown in (d).

patches at steady state is shown in Figure 1.2.

These out of phase solutions occur for a wide range of migrations as shown in Figure 1.2 (b, c), ranging several orders of magnitude, for any combination of (λ, γ), as long as parasitism (γ) is not large enough to result in overall extinctions. With increasing ϵ, we find that the length of the outbreaks decreases until the outbreaks occur for 1-2 generations. Further increasing ϵ, beyond this point leads to a transition towards in phase solutions, where the host outbreaks occur simultaneously in both patches (as shown in Figure 1.2 (d). We find that, the transition occurs in a very

small window for ϵ i.e., (in $0.01 < \epsilon < 0.025$). The exact nature and window of transition is complex and depends on other parameters i.e., λ and γ. These out of phase solutions are a result of small coupling and these oscillations differ greatly from when each of those oscillators are uncoupled, see Figure 1.2 (b, c) and Figure 1.2 (a), for comparison with individual uncoupled oscillators. Such emergence of new oscillations have been studied in detail in previous works with coupled oscillators as well [59], [51], although the out of phase solutions in these works were limited to period 2 cycles. The out of phase solutions in our work occur across a wide range of cycles, more of which we discuss in the section 5.

Out of phase solutions are further characterized by periods of near absence of hosts are accompanied by sudden outbreaks which last for few generations in each patch. However, if we look at the overall sum of host densities in both patches, they remain unchanging for most of the generations as shown in Figure 1.3 (a). However, the in phase solutions are different as periods of near absence of hosts are accompanied by sudden outbreaks lasting few generations, both at individual patch level and overall sum over both patches as shown in Figure 1.3 (b).

At higher values of ϵ, we see in phase solutions, where the peaks in host densities (i.e., host outbreaks) in 2 patches occur simultaneously (as shown in Figure 1.2 d) i.e., both patches oscillate in phase. High migration rates i.e., ($\epsilon \to 0.5$) lowers any difference in population in 2 patches. This happens till both patches oscillate in phase after which the effect of migration is negligible. To support this numerically observed result, we highlight below some analytical arguments to support why high migration leads to in phase solutions:

$$\begin{aligned} \Delta h_{t+1} &= h^1_{t+1} - h^2_{t+1} = \lambda(1-2\epsilon)\delta \\ \Delta p_{t+1} &= p^1_{t+1} - p^2_{t+1} \\ &= \gamma(1-2\epsilon)(\min(h^1_t, 1) - \min(h^2_t, 1) - \delta) \end{aligned} \tag{1.6}$$

where

$$\delta = \left(\min(h^1_t, 1)e^{-p^1_t} - \min(h^2_t, 1)e^{-p^2_t}\right)$$

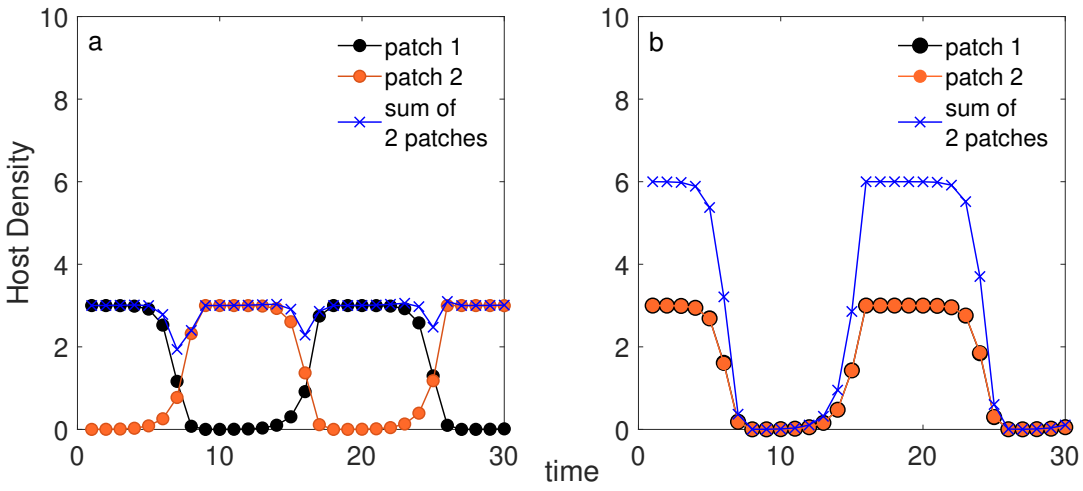

FIGURE 1.3. Host densities at steady state are shown for different migration rates. At low migration (a) i.e., $\epsilon = 10^{-6}$, we see that the host outbreaks in the 2 patches occur alternatively. The sum of the host densities remains constant with small fluctuations every few generations. In contrast, at high migration rates i.e. $\epsilon = 0.05$, host outbreaks in both the patches occur almost simultaneously as shown in b). We see cycles of large overall host outbreaks followed by generations of near host absence, as shown by the sum of the host densities in the 2 patches. The parameters used were $\lambda = 3$, $\gamma = 6$.

and $\Delta h_t, \Delta p_t$ represents the difference in host and parasitoid densities between patch 1 and 2 at time t. From Equation 6, we get:

$$\frac{\gamma}{\lambda}\Delta h_{t+1} + \Delta p_{t+1} = \gamma(1-2\epsilon)(\min(h_t^1, 1) - \min(h_t^2, 1)) \tag{1.7}$$

When both patches are undergoing buildup, $p_t^1 \approx p_t^2 \approx 0$ (see Supplementary Figure 1). Thus, we only focus on the difference in host densities, which without loss in generality, we assume $1 > h_t^1 > h_t^2$. Furthermore, when migration is high i.e., $\lambda(1-2\epsilon) < 1$, we have:

$$\Delta h_{t+1} < \Delta h_t$$

i.e., the difference between hosts in 2 patches keeps decreasing every generation during buildup. A similar argument can be formed when one patch is in outbreak and other is in buildup. Assuming $h_t^1 > 1 > h_t^2$ i.e., patch 1 is in outbreak and patch 2 is in buildup. Given parasitoid densities in both patches are still very low i.e., $p_t^1 \approx p_t^2 \approx 0$ (see Supplementary Figure 1), we again focus only on difference in host densities. When migration is high i.e., $\lambda(1-2\epsilon) < 1$, we have

$$\Delta h_{t+1} \approx \lambda(1-2\epsilon)(1-h_t^2) < \lambda(1-2\epsilon)\Delta h_t < \Delta h_t$$

i.e., the difference in host densities in 2 patches decreases. Furthermore, if both patches are in outbreaks, the host densities are in carrying capacity i.e., $h_t^1 = h_t^2 = \lambda \implies \Delta h_{t+1} = h_t = 0$, then from Equation 6, we see that

$$\Delta p_{t+1} = \gamma(1-2\epsilon)(e^{-p_t^2} - e^{-p_t^1})$$

Since parasitoid densities are still low i.e., $p_t^1 \approx p_t^2 \approx 0$, we can use Taylor expansion and have $e^{-p_t^2} - e^{-p_t^1} < p_t^1 - p_t^2 = \Delta p_t$ and that at high migration $\gamma(1-2\epsilon) < 1$, to get

$$\Delta p_{t+1} < \Delta p_t$$

i.e., the parasitoid densities decrease every generation as long as both patches are in outbreak. Lastly, we do not account for crashes or the small times during outbreaks when parasitoid densities are significant, typically the last generation of outbreaks. We know from numerical studies that these small times do not destroy the synchronizing behavior of migration during combined time of buildup and outbreak, for which we provided mathematical arguments above.

1.4. Robustness across choice of functions

TABLE 1.1. List of all different functions we've tested in our 2 patch model

Description	Mathematical form	Other parameters involved
Ricker map for hosts intraspecific competition	$F(H_t) = e^{r(1-\frac{H_t}{K})}$	Growth rate r, Carrying Capacity K
Smith map for hosts intraspecific competition	$F(H_t) = \frac{H_t}{1+(\lambda-1)(\frac{H}{K})^b}$	Growth factor λ, Carrying capacity K, strength of competition b
Independent search by parasitoids for hosts	$G(H_t, P_t) = e^{-aP_t}$	Per capita searching efficiency a
Aggregated attacks by parasitoids on hosts	$G(H_t, P_t) = \left(1 + \frac{aP(t)}{k}\right)^{-k}$	Per capita searching efficiency a, Degree of aggregation k

Our results from the previous section are robust across different choices of intraspecific competition i.e., $F(H_t)$ and parasitism $G(H_t, P_t)$. For $F(H_t)$, we chose Ricker map and a function described by Maynard Smith, for annual insects amongst choice of intraspecific competition (as shown in the

table below). For $G(H_t, P_t)$, we used both independent and aggregated parasitoid search for hosts.

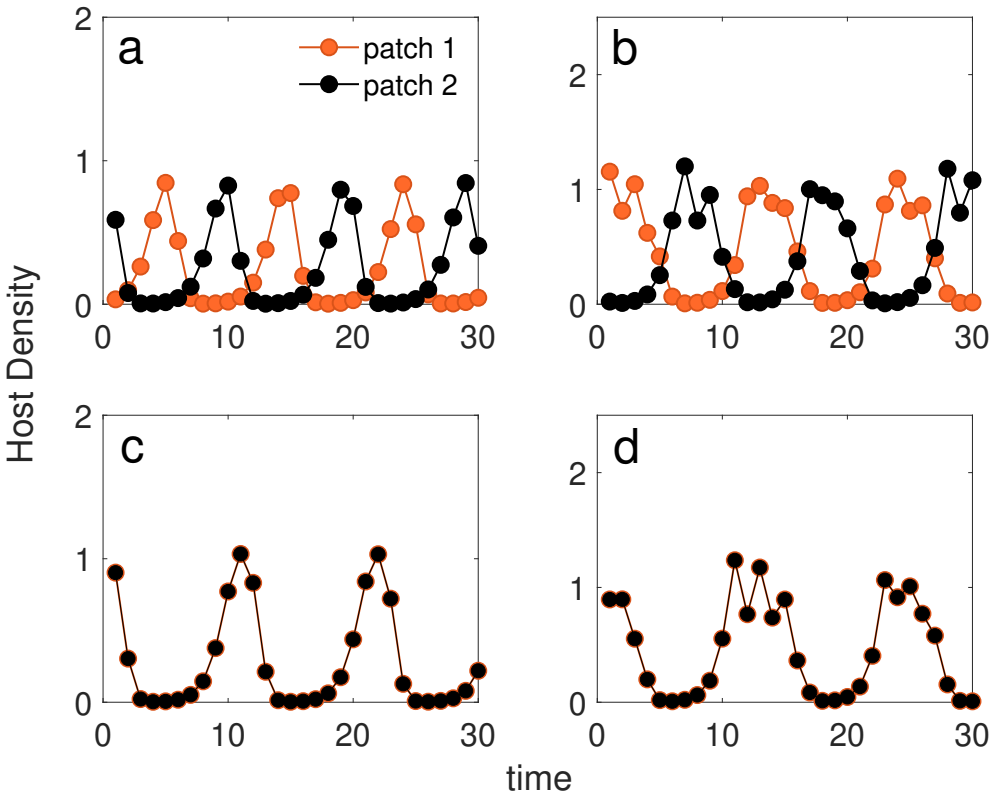

FIGURE 1.4. Host densities in 2 patches are plotted at steady state. Top (bottom) row represents cases for low (high) migration rates respectively. a) and c) are examples where host intraspecific competition was modelled using Ricker map and the parasitoid attack was aggregated. b) and d) are examples where intraspecific competition was modelled using Smith map and parasitoid search for hosts are independent.

We found similar out of phase and in phase oscillations at low and high values of migration for any combination of functions mentioned above. Figure 1.4 shows a few specific cases of our findings. In each modelling framework, the existence of out of phase and in phase solutions solely depends on the migration, across a range of other parameters involved in the modelling framework. This indicates that the synchrony patterns are robust across modelling choices, as long as intraspecific competition and parasitism are included in biologically relevant way. Migration is the determining factor for the resulting synchrony between the patches.

1.5. Length of the cycle

When migration rate is high, both patches oscillate in phase, behaving like a single patch. Thus, any measure of length of cycle i.e., time between successive host outbreaks, can be calculated using the equations derived for a single isolated patch [121]. We provide an approximate expression for length of cycle when migration rates are low and both patches oscillate out of phase. We assume that during out of phase oscillations the buildups and outbreaks occur in the two patches alternatively, without any overlap. This assumption is true for most of the out of phase oscillations we see in our model with few exceptions (where there's partial overlap between buildups and outbreaks). We define $T_{\mathrm{b},i}$, $T_{\mathrm{o},i}$ and $T_{\mathrm{c},i}$ as the number of generations patch i undergoes buildup, outbreak and crash respectively. Following the assumption about out of phase oscillations, we can conclude the following (without losing generality):

- Duration of buildup in 1 patch must be no more than the combined duration of outbreak and crash in patch 2 i.e.,

$$T_{\mathrm{b},1} \leq T_{\mathrm{o},2} + T_{\mathrm{c},2} \tag{1.8}$$

  If this condition isn't satisfied, then both the patches will have build-up simultaneously, which isn't the case in out of phase oscillations.

- Duration of buildup in 1 patch must be no less than the duration of outbreak in patch 2 i.e.,

$$T_{\mathrm{b},1} > T_{\mathrm{o},2} \tag{1.9}$$

  If this condition isn't satisfied, then both the patches will have outbreaks simultaneously, which isn't the case in out of phase solutions.

Since typically a crash occurs for 2-3 generations in our model, as shown in [121], we have $T_{\mathrm{c},2} =$ 2 or 3. For the rest of the analysis, we assume $T_{\mathrm{c},2} = 2$, as this provides an upper bound on $T_{\mathrm{b},1}$ for Equation 8, which holds whether the crash is 2 or 3 generations long. If we take $T_{\mathrm{c},2} = 3$ to derive the upper bound on $T_{\mathrm{b},1}$, then the buildups will overlap following the cycles when the crash only lasts 2 generations long, which is not how we define out of phase solutions. Taking $T_{\mathrm{c},2} = 2$ gives

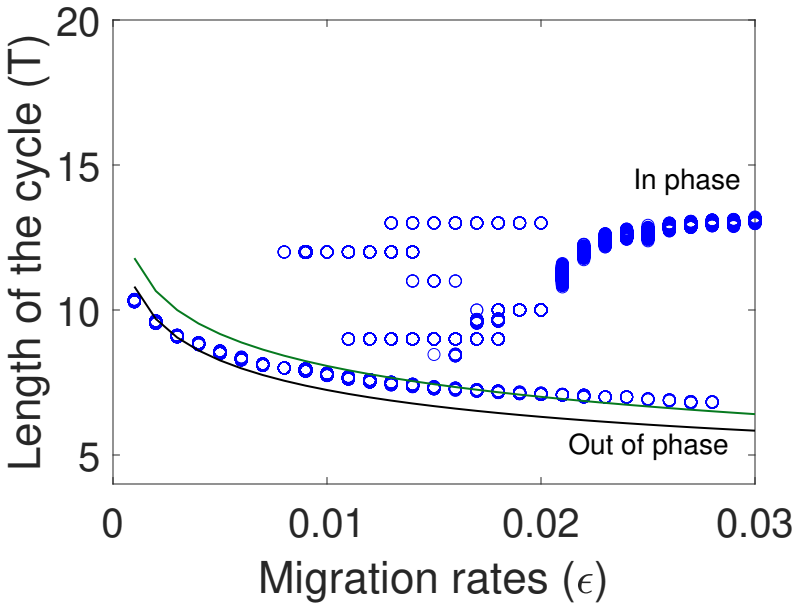

FIGURE 1.5. Length of cycle (numerically and approximate expressions - Equation 18 (black) and Equation 21 (green)) are plotted. Each blue dot represents length of cycle numerically obtained for a single iteration, after taking the mean of 1000 different cycles at various time points (randomly selected) after steady state was reached. The green and black curves represent the approximate theoretical expressions for length of a cycle when both patches are out of phase, as derived in the text. When $\epsilon < 0.01$, we mostly get out of phase solutions which changes as ϵ is increased. At higher migration i.e., $\epsilon > 0.02$, although most of our simulations result in both patches oscillating in phase, we still find some cases where both patches oscillate out of phase. Our theoretical expressions for length of cycle of out of phase solutions matches the numerically obtained ones even at high migration values, where the occurrences of out of phase solutions are few. Here $\lambda = 3.375$ and $\gamma = 4.875$.

us solutions which always ensure the buildups occur alternatively. Combining Equation 8 and 9, with the fact that $T_{c,2} = 2$, we get the expression

$$T_{b,1} = T_{o,2} + 1 \text{ or } 2 \tag{1.10}$$

Because both the patches are symmetric, we have $T_{b,1} = T_{b,2}$ and $T_{o,1} = T_{o,2}$. Henceforth, we will drop the patch numbers and just talk about buildup (T_b), outbreak (T_o) and crash (T_c) phases and the total length of the cycle (T).

$$T = T_b + T_o + T_c \tag{1.11}$$

Substituting T_b from Equation 10 in Equation 11 and adding that $T_c = 2$, we get

$$T = 2T_o + 3 \text{ or } 2T_o + 4 \tag{1.12}$$

In a single isolated patch, the host density after a crash is given by $H = \lambda^2 e^{-\gamma\left(2-\frac{1}{\lambda}\right)}$ (as shown in [121]). In our 2 patch model, we assume that the host density after the crash (in patch 1) is changed only by the amount that is migrated by the patch 2. Since the patch 2 is in outbreak, the host density that migrated to patch 1 is given by $\epsilon\lambda$. Thus, the overall host density in patch 1 in the first generation of buildup is $H_1 = \lambda^2 e^{-\gamma\left(2-\frac{1}{\lambda}\right)} + \epsilon\lambda$. Since γ is usually large, $\lambda^2 e^{-\gamma\left(2-\frac{1}{\lambda}\right)} \approx 0$. This is supported by the intuition that after the crash, the host densities are reduced to very small values due to parasitism. Thus, for very small values of migration i.e., $\epsilon \leq \lambda e^{-\gamma\left(2-\frac{1}{\lambda}\right)}$, we don't see any effect of migration and the two patches behave as if they are isolated patches. But for $1 >> \epsilon >> \lambda e^{-\gamma\left(2-\frac{1}{\lambda}\right)}$, $H_1 \approx \epsilon\lambda$. Given the geometric nature of the growth of host density during buildup (as parasitoid density is low, leading to no mortality due to parasitism) in addition to host migration from the other patch undergoing an outbreak, after t generations, we have

$$H_t = \epsilon(\lambda^t + \lambda^{t-1} + \cdots + \lambda) = \epsilon\lambda\frac{(\lambda^t - 1)}{\lambda - 1} \tag{1.13}$$

As long as the patch 2 is undergoing outbreak, the host density in the patch 1 in the buildup phase will continue to grow according to the expression above.

$$H_{T_o} = \epsilon\lambda\frac{(\lambda^{T_o} - 1)}{\lambda - 1} \tag{1.14}$$

Following outbreak, the patch 2 undergoes crash which has high parasitoid density, reducing host densities in that patch. Thus, we can ignore the effect of migration for the remainder of the buildup in patch 1, which can last 1 or 2 more generations (see Equation 10). Assuming the buildup in patch 1 lasted 2 more generations after outbreak in patch 2, we get the following

$$H_{T_b} = \epsilon\lambda^3\frac{(\lambda^{T_o} - 1)}{\lambda - 1} \tag{1.15}$$

Similarly, at the end of buildup the host density is $H_{T_b} \approx 1$ (as shown in [121]). Equating the expected host densities at the start of outbreak, we get

$$\epsilon\lambda^3\frac{\left(\lambda^{T_o}-1\right)}{\lambda-1}\approx 1 \tag{1.16}$$

This gives us an approximate expression for T_o and $T = 2T_o + 4$ as follows

$$T_o = \frac{\ln\left(1+\frac{\lambda-1}{\epsilon\lambda^3}\right)}{\ln(\lambda)} \tag{1.17}$$

$$T = 4 + 2\frac{\ln\left(1+\frac{\lambda-1}{\epsilon\lambda^3}\right)}{\ln(\lambda)} \tag{1.18}$$

Furthermore, if instead we assume that the buildup in patch 1 lasted 1 more generation following outbreak in patch 2, in which case $T = 2T_o + 3$, we get the approximate expression as

$$H_{T_b} = \epsilon\lambda^2\frac{\left(\lambda^{T_o}-1\right)}{\lambda-1}\approx 1 \tag{1.19}$$

$$T_o = \frac{\ln\left(1+\frac{\lambda-1}{\epsilon\lambda^2}\right)}{\ln(\lambda)} \tag{1.20}$$

$$T = 3 + 2\frac{\ln\left(1+\frac{\lambda-1}{\epsilon\lambda^2}\right)}{\ln(\lambda)} \tag{1.21}$$

We've used the host dynamics to calculate the cycle length, hence the final expression doesn't have any dependence on γ. Parasitoid exclusion until the last stage of outbreak doesn't significantly affect the host densities as shown here [121] and supported by empirical evidence [120]. Our expression is approximate (as we've assumed $T_c = 2$) and could be improved with the inclusion of parasitoid dynamics as well. To test our expressions against numerical simulations, we plot them against the length of cycle numerically observed in out of phase solutions for different migration rates (for fixed λ and γ). To find the length of the cycle numerically, we measure the number of generations between peak parasitism (during crash) within each patch, after steady state is reached, which occurs after few 100 generations. We measure this 1000 times from either patch at random times after steady state is reached, to account for minor variations in the length of cycle after steady state is reached. The length of the cycle is the mean of these 1000 instances. Furthermore, for each value of ϵ, we repeat this for 10,000 different iterations, with different initial conditions,

to account for any dependency on initial conditions. Complex dependency of synchrony on initial conditions have been shown in discrete time coupled oscillators in previous works before [59], [4]. Our studies differ from those as we focus on length of cycle to show the dependency on initial conditions, instead of basin of attraction and bifurcation diagrams (done in previous studies) as obtaining those for our system is complex.

We plot the length of a cycle for all of these 10,000 iterations (for a given ϵ) in the same plot. When $\epsilon \approx 0$ or $\epsilon \approx 1$, the length of cycle should be same as that of a single isolated patch, hence we focus on when ϵ is far from those extremes. Within the range of values leading to out of phase solution ($0.001 \leq \epsilon < 0.008$ in Figure 1.5), increasing ϵ increases the degree of recolonization to the patch with low host density, thus leading to sooner more frequent outbreaks, hence a decrease in length of cycle. We see the length of cycle decreases from approximately 10 to 6 as ϵ is increased from 0.001 to 0.028. The exact changes in length of cycles depends on the values of λ and ϵ, as predicted by the Equation 18 and 21 and thus can incorporate a larger range of out of phase solutions than the 2 cycle solutions studied in [59], [51]. Furthermore at low migration i.e., for $\epsilon < 0.008$, we only find out of phase solutions as long as initial conditions in both patches aren't identical, unlike continuous time weakly coupled oscillators where you get multiple stable states (other than an out of phase and an in phase solution) at low coupling [49], [126].

As ϵ is increased beyond 0.008, we start to see emergence of other stable solutions making the final state of the system dependent on initial conditions. Increasing ϵ beyond 0.02, we mostly get in phase solutions, with some out of phase solutions as well which are less common, dependent on the initial conditions. Our analytical expressions derived in Equation 18 and 21 (shown in green and black in Figure 1.5) for out of phase solution matches the numerically obtained length of cycle for out of phase solutions, even at higher ϵ when out of phase solutions are rare.

1.6. Cellular Automata model

In this section, we show that our main result - patches oscillating out of phase at low migration rates and in phase at higher migration rates - is independent of the exact biological details of our

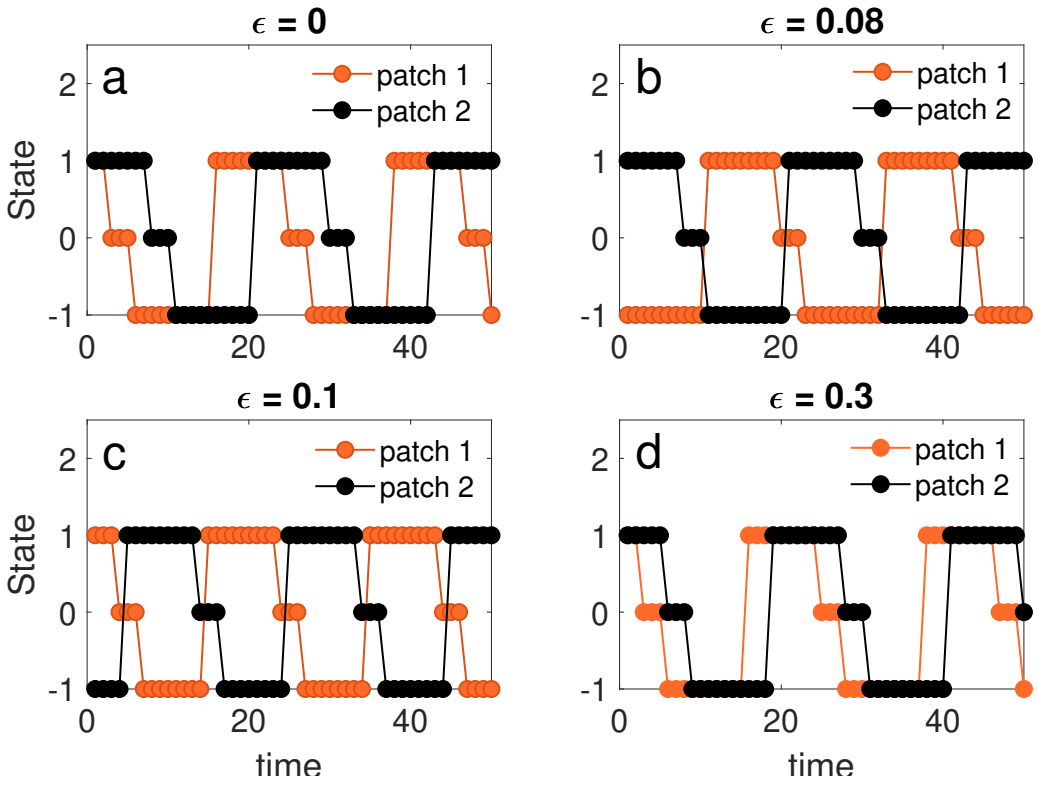

FIGURE 1.6. An example of the results for different migration rates from our cellular automata model is shown. Here m = 10, n = 9, o = 3. State 1 represents outbreak, state 0 represents crash and state -1 represents buildup. a) migration rate is 0 and hence both patches oscillate independently. At intermediate values of migration ((b) and (c)), we see both patches out of phase. At higher values of migration i.e., (d), we see both patches closer to being in phase.

modelling of host parasitoid system. Higher migration rates imply greater reduction in any difference in densities between the patches. Hence, it's not surprising that the result - patches oscillating in phase at higher migration rates - would hold independent of exact biological modelling details of the host parasitoid system. We instead focus on cases when migration rates are low, exact biological details are ignored and instead a cellular automata model is considered. We show that out of phase solutions arise at low migration rates in our cellular automata model, and show a shift towards in phase solutions as migration rates are increased (see Figure 1.6). Our cellular automata model is rooted in the empirical observation common to many insect outbreaks i.e., insect densities stay at low densities for many years before outbreaking at high densities [78]. Hence, without going into the biological details of it we assume that the buildup occurs for m generations followed by outbreak for n generations and then crash for o generations (and the cycle continues). The

state of the host-parasitoid system in a patch can be written as a variable k, indicating how many generations have passed since the start of the cycle, such that $1 \leq k \leq m + n + o$. In an isolated patch, this state variable k increases by 1 every generation until the end of the cycle is reached i.e., $k = m + n + o$, after which it resets to 1, indicating start of a new cycle.

Now we consider 2 patches at a given time t, patch 1 is in state $k_{1,t}$ and patch 2 in state $k_{2,t}$, with diffusive migration between them. Earlier in our two patch model with explicit biological details of host and parasitoid, effect of migration was significant in 2 scenarios i.e., 1) when one patch was in buildup, other in outbreak, leading to significant changes in host densities in the patch undergoing buildup and 2) when one patch is in outbreak, other in crash, leading to significant changes in parasitoid densities in the patch undergoing outbreak. Incorporating those features in the 2 patch dynamics of our cellular automata model, the rules are as follows (same rules apply if the states of patches 1 and 2 are reversed):

- If patch 1 is in buildup ($1 \leq k_{1,t} \leq m$) and patch 2 is in outbreak ($m < k_{2,t} \leq m + n$), then the state of patch 1 in the next generation is given by $k_{1,t+1} = k_{1,t} + \epsilon(k_{2,t} - k_{1,t})$ rounded to the next integer. This is supported by the intuition that the changes due to migration would be dependent on the difference in the current states of the two patches. The state of patch 2 in the next generation increases as usual i.e., $k_{2,t} = k_{2,t} + 1$. This is supported by the biological intuition that when migration is low, the host and parasitoid densities in the patch undergoing outbreak doesn't change significantly.
- If patch 1 is in outbreak ($m < k_{1,t} \leq m + n$) and patch 2 is in crash ($m + n < k_{2,t} \leq m + n + o$), then the state of patch 1 in the next generation is given by $k_{1,t+1} = k_{1,t} + \epsilon(k_{2,t} - k_{1,t})$ rounded to the next integer. Just like before, this is supported by the intuition that the changes due to migration would be dependent on the difference in the current states of the two patches. The state of patch 2 in the next generation increases as usual i.e., $k_{2,t} = k_{2,t} + 1$. This is supported by the biological intuition that when migration is low, the parasitoid densities in the patch undergoing crash doesn't change significantly. Furthermore, any host migration doesn't change the host densities in either patch significantly because patch 1 undergoing outbreak is already at maximum host density and

patch 2 undergoing crash has high parasitoid density, which would kill any hosts migrating into this patch.

- In all other scenarios, patches 1 and 2 behave as if they are isolated i.e., k_1, k_2 increases by 1 every generation.

Figure 1.6 shows the results for different values of migration. Similar to the cases in host-parasitoid system with explicit biological detail, when $\epsilon = 0$, both patches have no change in their state due to migration. At low migration values, we see both patches oscillate out of phase, which changes at higher migration rates. We used m = 10, n = 9 and o = 3 for our figure. But our results are valid for many values of m, n and o as long as m $\approx$ n >> o. This is an important condition because crash is often short-lived compared to buildup or outbreak phases.

1.7. Discussion and Conclusion

Understanding spatial synchrony in foliage eating insect outbreaks has been a long standing problem in ecology [78]. Since the simplest spatial model has 2 locations, several discrete time 2 patch models have been studied to understand these spatial processes. We replicate some of the results from those studies and add new interesting insights into the literature. Specifically, we show the existence of out of phase solutions at low migration values, which was shown before [4]. However, the earlier model lacked important stabilizing factors and the parasitism was modelled similar to the classical Nicholson-Bailey model, without any density dependence in host. Outbreaking insect herbivores are often resource limited and thus including such interactions can be key to understanding the overall emergent dynamics. Density dependent factors can have complex stabilizing or destabilizing effects in the presence of migration as shown previously in [95], [74]. Furthermore, parasitoids have different foraging behaviors ranging from independent search for hosts throughout the area [99], to aggregated search for favorable hosts [93]. Thus, we surveyed the literature of host-parasitoid systems [24], [56] and used a suite of different functional forms to model intraspecific competition for resources among hosts and parasitism. Our analysis shows that the result that two patches oscillate out of phase when migration is low, is robust across the modelling choices for intraspecific competition and parasitism. Robustness across modelling choices is useful whenever direct comparison with data is lacking or difficult, which is the case in host parasitoid populations

as most time series data for insect outbreaks are about 20-30 years long, which is inadequate for testing properties of these cycles [78]. Our robustness to modelling choices also presents avenues of further analytical work where this robustness is mathematically shown starting from a modified version of Eq. (1).

Our analysis of discrete time equations is significantly different from previous work on discrete coupled oscillators [51], [59], [107], where much of the emphasis was on persistence of solutions and the use of bifurcation diagrams to understand stability and equilibrium. Since outbreaking insects are not in equilibrium, equilibrium analyses cannot be directly applied here. Instead, we focus our attention on finding the length of cycle, which corresponds to how often the outbreaks occur. The benefit of doing this is two fold. Length of cycle is a statistic that could be compared to real world data, even if the data is limited, as opposed to asymptotic equilibrium states which most natural systems are far from. Secondly, plotting length of cycles numerically for different migration rates reveals the richness of our system, in terms of both existence of multiple solutions and the system's dependence on initial conditions. Using some assumptions, we show how to derive an analytical expression for length of a cycle (Eq. (8-21)), when the two patches oscillate out of phase. Our approach is different from the standard analyses, where the underlying model is linearized and eigenvalues are calculated. We used approximations grounded in our understanding of different stages (i.e., buildup, outbreak and crash) that are characteristic of insect outbreaks [121]. We found that our theoretical expressions are in agreement with the simulation results (Figure 1.5), even at higher migration, where out of phase solutions are the less dominant solution. In the range of migration where out of phase solutions occur most commonly, increasing migration decreases cycle length (from 10 - 6 in Figure 1.5), matching our intuition that greater recolonization would lead to more frequent outbreaks. The range of cycle length emerging in our analysis matches some of the empirical data as shown by [18]. Furthermore, at intermediate values of migration, we see existence of multiple solutions, indicating the system's sensitivity to initial conditions. This sensitive dependence on initial conditions is an important lesson for ecologists as it arises due to non-linear dynamics inherent in coupled oscillators [75], [59].

Our study supplements the large body of coupled discrete time models, which aim to study spatial synchrony and population oscillations. We assume that competition, migration, parasitism and reproduction are separated in time, an assumption that holds for egg and pupal parasitoids. For species where there is overlap amongst these processes, continuous time models are better suited. In addition, if the time step between successive generations becomes very small, our system converges to a continuous time predator prey system. Synchronization amongst predator prey models in continuous time is well studied [49], [126]. Existence of multiple phase locking solutions and dependence on initial conditions are some of the features that our results on cycle length share with continuous time models. While previous works have shown how out of phase solutions loses stability as migration is increased, we also show how the cycle length for out of phase solutions decrease in the process, which is novel. We also predict that the cycle length shown in Figure 1.5 will approach a bifurcation diagram, where the stable solution transitions from out of phase to in phase branches as migration is increased.

Lastly, we also asked if such oscillations are rooted in the specific biological details of a host-parasitoid system. We use a 3 state cellular automata model devoid of any biological details (like competition, parasitism etc.), which qualitatively undergoes buildup, outbreak and crash for m, n and o time steps respectively. This is rooted in the empirical studies on the time series of many insect observations, which remain in very low densities for many years before outbreaking (and the cycle continues). We show that as long as $m \approx n >> o$, the two patches oscillate out of phase when migration is low (Figure 1.6). Our assumption $m \approx n >> o$ translates to the fact that the hosts either stay at very low densities or are outbreaking and the transition between them is fast, within 1-2 generations, which is appropriate for many observed insect oscillations. Generations in which parasitoids impact host numbers significantly is very small compared to the time of buildup or outbreak, supported by empirical studies [18]. Within the assumptions of our cellular automata model, migration determines whether the two patches oscillate out of phase, in phase or somewhere in between. Although similar cellular automata models have been used in studies before (see [58]), our work presents new insights. Our analysis shows that out of phase oscillations could arise as long as the population in each patch undergoes a cycle of 3 stages, where one stage (i.e., crash) is much smaller than the other two (buildup and outbreak). This result could hold true for populations

other than host-parasitoid system, which have large amplitude oscillations and have many years of near absence followed by outbreaks. Our results won't hold for more general oscillations where the transitions between buildup and outbreaks are gradual, and the condition that m $\approx$ n $>>$ o doesn't hold. Our work could be extended to a more general framework which could map oscillations across patches to oscillations in individual patches, a problem which is of interest in metapopulation studies.

CHAPTER 2

Effect of Spatial Heterogeneity in Spatial Metapopulation models

Abstract

Metapopulation models are widely used in spatial ecology to understand how dispersal, local interactions, and spatial structure influence population dynamics. However, such models often rely on simplifying assumptions - uniform habitat patches and periodic boundary conditions - that rarely reflect the complexity of real ecosystems. In this study, we explore the consequences of these assumptions using a discrete-time host-parasitoid model on a two-dimensional lattice, with migration between adjacent patches. We introduce landscape heterogeneity by randomly designating a fraction of patches as uninhabitable and impose either absorbing or reflecting conditions near these uninhabitable patches and lattice boundaries. We examine the relationship between steady-state host density and migration rate across different levels of heterogeneity and migration values. Our results reveal three qualitatively distinct spatial regimes: asynchronous local oscillations at low migration, synchronized landscape-wide outbreaks at intermediate migration, and a novel spiral wave phase at high migration in heterogeneous landscapes, where wavefronts emerge from an interplay between landscape heterogeneity and local population dynamics - distinct from wave-generating mechanisms in previous models. These spatial regimes are further characterized using pairwise temporal correlations between neighboring patches. Notably, we show that even small degrees of heterogeneity can lead to dramatic reductions in host density and a qualitative shift in the emerging spatial structure - effects that arise not solely from migration-induced mortality, but from fundamental changes in spatial population dynamics. Our findings highlight the importance of explicitly incorporating heterogeneity in spatial ecological models and caution against relying solely on idealized homogeneous landscapes when interpreting migration effects in real systems.

2.1. Introduction

Understanding how spatial structure and movement shape population dynamics remains a central challenge in theoretical ecology [85]. In systems where local populations are coupled through dispersal - whether through active movement, migration, or passive transport - spatial interactions can stabilize or destabilize dynamics, generate large-scale synchrony, and shape patterns of persistence and extinction [1]. Classic examples include predator-prey and host-parasitoid systems, where dispersal can influence the size and duration of insect outbreaks, and determine spatial patterning across landscapes [24, 58]; epidemic spread, where host movement influences outbreak synchrony and wavelike infection fronts [50,80]; invasive species, where dispersal across fragmented landscapes determines range expansion and control outcomes [97, 133]; and metacommunity models, where movement across habitat patches shapes biodiversity and community stability [83]. Across these systems, spatial coupling plays a key role in driving ecological patterns at both local and regional scales.

To explore the complex relationship between movement and emerging population dynamics, metapopulation models and other spatial population models have become a cornerstone of spatial ecology. These models represent landscapes as discrete habitat patches, within which local dynamics unfold and between which individuals migrate. Such frameworks have yielded critical insights into how dispersal shapes extinction risk, recolonization dynamics, regional persistence, and spatial synchrony [55, 58, 61, 84, 102, 118]. For analytical tractability, however, many spatial ecological models assume homogeneous habitat quality and periodic boundary conditions - simplifications that, while useful, can obscure the ecological consequences of real-world spatial heterogeneity.

In natural landscapes, habitat quality is rarely uniform, and sharp boundaries, uninhabitable patches, and patch-level variation are the norm. Spatial heterogeneity, including forms of habitat loss and fragmentation, can profoundly influence population persistence, synchrony, and spatial patterning [40, 133]. Neutral landscape models (NLMs) have played a key role in formalizing how structural variation in habitat layout affects ecological dynamics [129,134]. These models highlight that even modest changes in habitat distribution can shift core relationships between population density, dispersal, and persistence. Despite this, many classical spatial ecological models have not

examined whether the relationships they uncover, like between migration rate and steady-state population density, remain valid under even small-scale heterogeneity.

In this study, we ask: How robust are the ecological insights derived from idealized spatial ecological models when small amounts of spatial heterogeneity are introduced? Intuitively, one might expect that minor habitat loss - such as a small fraction of uninhabitable patches scattered across the landscape - should not dramatically alter the overall system dynamics. If most patches remain habitable and connected, why should a few structural imperfections lead to significant changes in population patterns or synchrony? Moreover, how do behavioral responses to these uninhabitable patches affect the outcome? In particular, we explore two contrasting movement rules near heterogeneities: an *absorbing* case, where individuals disperse blindly into uninhabitable patches and are lost (representing migration-induced mortality), and a *reflecting* case, where individuals can detect and avoid uninhabitable patches, thereby eliminating mortality during dispersal. This allows us to disentangle the structural effects of heterogeneity from the demographic effects of dispersal loss.
To answer these questions, we begin by reviewing previously studied models of single and two-patch host-parasitoid dynamics, which form the foundation of our spatially explicit framework. We then extend those to a spatial model on a square lattice, where each patch contains a host-parasitoid system. Spatial heterogeneity is introduced in a simple ecologically meaningful way: by randomly designating a small fraction of patches η as uninhabitable. We simulate localized habitat loss while preserving large-scale connectivity. The landscape also includes sharp boundaries, limiting dispersal to within the grid. Finally, we compare absorbing and reflecting movement rules near heterogeneities to isolate the role of migration-induced mortality in shaping spatial outcomes.

2.2. Host-Parasitoid dynamics in Single and Two-Patch Systems

We base our model on well-established formulations for host-parasitoid population dynamics, following [92], in which three sequential phenological stages are modeled: reproduction, intraspecific competition between hosts, and parasitism by parasitoids. These processes determine the annual densities of hosts (H_t) and parasitoids (P_t), which evolve according to the following general form:

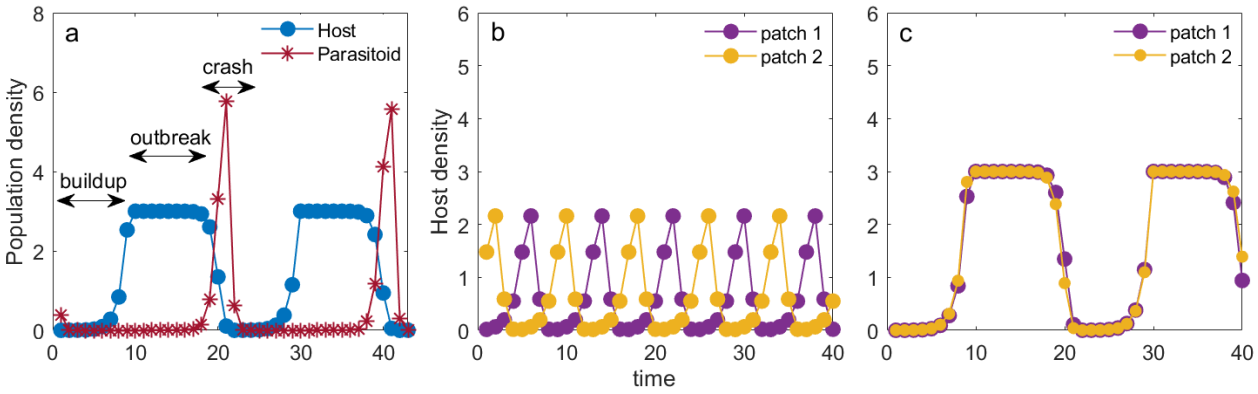

FIGURE 2.1. Time series illustrating host-parasitoid dynamics at steady state, adapted from previous studies. (a) A single isolated host-parasitoid patch exhibits characteristic cyclic dynamics marked by three distinct phases—initial buildup of hosts, rapid host population outbreak, and subsequent crash due to intense parasitoid activity. These phases repeat indefinitely in the absence of spatial interactions [121]. (b–c) When two identical patches are connected by migration, the degree of migration fraction (ϵ) influences synchronization of their host dynamics [82]. (b) At low migration ($\epsilon = 0.01$), host populations oscillate asynchronously, resulting in out-of-phase local dynamics. (c) At higher migration ($\epsilon = 0.3$), synchronization emerges, leading to in-phase oscillations in host densities across connected patches.

$$H_{t+1} = \lambda\, F(H_t)\, G(H_t, P_t)$$

$$P_{t+1} = c\, F(H_t)(1 - G(H_t, P_t)) \tag{2.1}$$

Here, λ is the intrinsic growth rate of the hosts, and c is the number of parasitoids emerging from a single parasitized larva. Following the approach in [121], we reduce the system to a non-dimensional form (Equation 2). The min function is used to model the effects of intraspecific host competition, which is exactly compensating. This dynamical system lacks a stable fixed point and thus exhibits persistent oscillations in both host and parasitoid densities, as shown in Figure 2.1a.

$$h_{t+1} = \lambda \min(h_t, 1)\, e^{-p_t}$$

$$p_{t+1} = \gamma \min(h_t, 1)(1 - e^{-p_t}) \tag{2.2}$$

These oscillations consist of three distinct stages that repeat indefinitely (see Figure 2.1 a):

(1) Buildup – host and parasitoid densities are low; the effects of competition and parasitism are negligible.

(2) Outbreak – host density is high while parasitoid numbers remain low. host abundance leads to rapid growth of parasitoids.

(3) Crash – parasitoids reach high densities and substantially reduce host numbers over 2-3 generations.

When two such patches are connected by migration, where a fraction ϵ of both host and parasitoid populations migrate between patches each generation, the patches are synchronized [82]. The degree of synchrony between the patches depends strongly on ϵ. At low ϵ, the patches oscillate out of phase, with host outbreaks occurring alternatively (Figure 2.1b). As ϵ increases, the dynamics of the two patches gradually synchronize. At high ϵ, host populations in both patches oscillate in phase and the system behaves similarly to a single well-mixed patch (Figure 2.1c).

This transition from out-of-phase to in-phase oscillations with increasing migration has been observed across various host-parasitoid models, as long as the three key biological processes - reproduction, competition, and parasitism - are represented [82]. This robustness makes single-patch dynamics a natural building block for constructing larger metapopulation models, which we explore in subsequent sections.

2.3. Spatially explicit metapopulation model

We extend the local host-parasitoid model (Equation 2) to a spatial metapopulation framework consisting of $N = L^2$ habitat patches arranged on a two-dimensional square lattice of size $L \times L$. Each patch hosts a local population governed by the same phenological structure as in the single-patch case. After each generation of within-patch dynamics, a fraction ϵ of the host and parasitoid populations migrates to the four nearest neighboring patches (von Neumann neighborhood), as described by Equation 3.

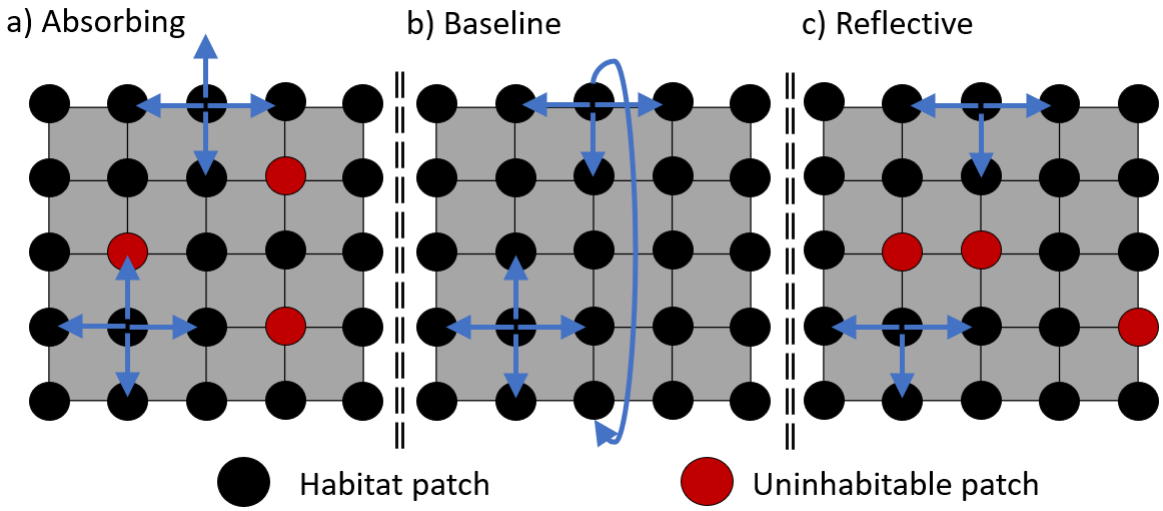

FIGURE 2.2. Schematic representation of the three landscape boundary scenarios considered in this study, illustrating migration from two example habitat patches—one located within the landscape, and one at its boundary. In (a) the *absorbing* landscape, populations migrate indiscriminately and cannot detect boundaries or uninhabitable patches (red circles), resulting in mortality when migrating into these areas. In (b) the *baseline* landscape, all patches are habitable and periodic boundary conditions apply; populations migrating beyond one boundary re-enter from the opposite side, as illustrated by the looping arrow. In (c) the *reflecting* landscape, populations sense and actively avoid migrating into uninhabitable patches and boundaries, restricting their migration to habitable regions only. Black circles represent habitable patches, and red circles represent randomly distributed uninhabitable patches.

$$
\begin{aligned}
h_i &= \lambda \min(h_{t,i}, 1)\, e^{-p_{t,i}} \\
p_i &= \gamma \min(h_{t,i}, 1)(1 - e^{-p_{t,i}}) \\
h_{t+1,i} &= (1-\epsilon)\, h_i + \frac{\epsilon}{4} \sum_{<i,j>} h_j \\
p_{t+1,i} &= (1-\epsilon)\, p_i + \frac{\epsilon}{4} \sum_{<i,j>} p_j
\end{aligned}
\tag{2.3}
$$

In typical metapopulation studies, all patches are assumed to be identical and habitable, and the landscape is wrapped with periodic boundary conditions. Individuals migrating out of one edge re-enter the landscape from the opposite edge (Figure 2.2b). In contrast, we introduce spatial heterogeneity and sharp boundaries into the system to more realistically capture ecological structure.

Specifically, we randomly designate a fraction η of patches as uninhabitable. Populations migrating into these patches cannot persist. The landscape is bounded, and habitat patches are confined strictly within the grid (Figures 2.2a,c).

To model behavior near boundaries and uninhabitable patches, we consider two distinct types of migration responses:

(1) **Absorbing conditions** – Populations are unaware of boundaries or uninhabitable patches and may migrate into them, resulting in mortality.

(2) **Reflecting conditions** – Populations detect uninhabitable patches and boundaries and avoid migrating into them. Migration occurs only between habitable patches, so there is no migration-induced mortality.

Each simulation replicate is initialized by setting host densities to their carrying capacity in all habitable patches, and introducing a small parasitoid population into a single randomly selected habitable patch (Figure 2.6a). All patches update synchronously, reflecting annual lifecycles of these populations. The system is evolved for 5000 generations, with the first 4000 generations discarded as transients. Steady-state statistics are computed by averaging over the final 1000 generations. To ensure robustness, we repeat this simulation over 1920 independent landscape realizations for each parameter set, varying both the spatial configuration of uninhabitable patches and the location of initial parasitoid introduction.

For each of the 1920 simulation replicates, we simulated the system under four levels of heterogeneity: $\eta = 0$, 0.01, 0.05, and 0.1, corresponding to 0%, 1%, 5%, and 10% of patches (rounded to the nearest integer) being uninhabitable. To maintain consistency across these four cases within a given replicate, we ensured that the uninhabitable patches in each landscape were nested such that the $\eta = 0.01$ landscape was a strict subset of the $\eta = 0.05$ landscape, which in turn was a subset of the $\eta = 0.1$ landscape. Additionally, the initial parasitoid introduction occurred at the same randomly selected habitat patch across all four heterogeneity levels within each replicate. This controlled structure allows for a consistent comparison of how increasing heterogeneity affects population dynamics while minimizing variability due to spatial configuration and location choices of parasitoid introduction. The $\eta = 0$ case serves as our homogeneous reference landscape, which

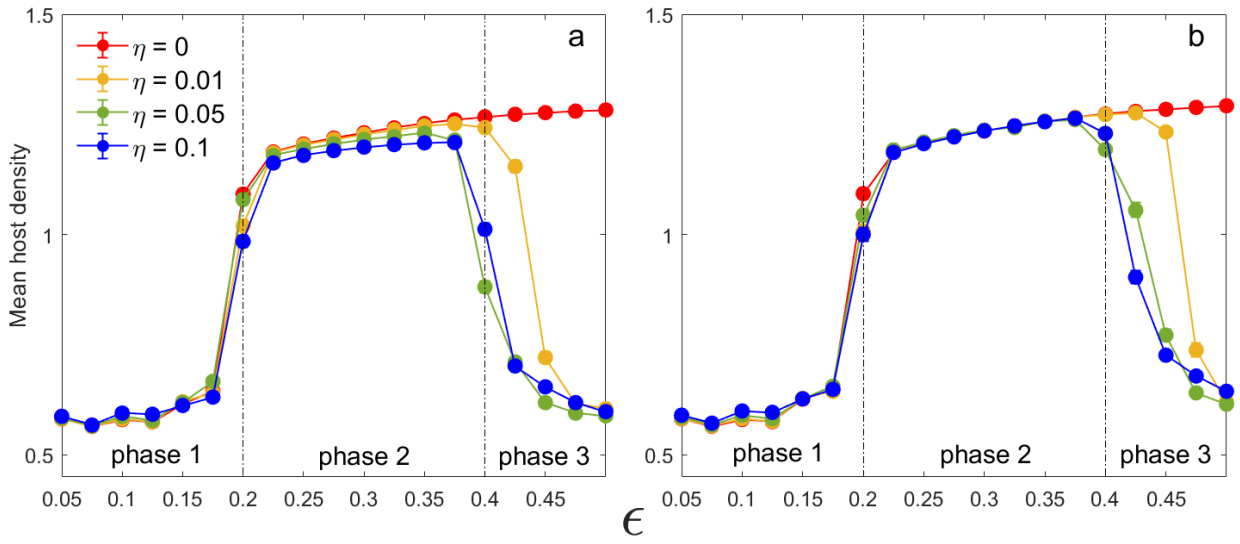

FIGURE 2.3. Mean steady-state host densities as a function of migration fraction (ϵ) for (a) absorbing and (b) reflecting boundary conditions, across varying levels of landscape heterogeneity (η). Here, $\eta = 0$ (red) corresponds to landscapes without uninhabitable patches, while $\eta = 0.01$ (yellow), $\eta = 0.05$ (green), and $\eta = 0.1$ (blue) represent landscapes containing 1%, 5%, and 10% randomly distributed uninhabitable patches, respectively. Error bars indicate 95% confidence intervals obtained from bootstrap resampling, and are often smaller than markers. Vertical dashed lines indicate approximate locations of qualitative shifts in the system dynamics, dividing the dynamics into three distinct phases. At low migration (Phase 1), mean host densities remain low due to asynchronous local dynamics. Intermediate migration rates (Phase 2) lead to spatially synchronized host outbreaks and substantially increased host densities. At higher migration (Phase 3), mean host densities remain high in homogeneous landscapes ($\eta = 0$), whereas heterogeneous landscapes exhibit a marked decrease due to the emergence of persistent traveling wave patterns (as illustrated in Figure 2.5). This highlights how even small landscape heterogeneities can profoundly impact spatial synchronization and host-parasitoid dynamics, particularly at higher migration rates.

still incorporates absorbing or reflecting boundaries. We present the results from our models by setting $L = 128$, $\lambda = 3$, and $\gamma = 6$, although our qualitative results remain robust across a broad range of parameter choices.

We primarily focus on models with heterogeneity ($\eta > 0$) and sharp boundaries. We also simulate baseline scenario with periodic boundaries and no uninhabitable patches (shown in Figure 2.2 (b)). A direct comparison between this scenario and results from $\eta = 0$, with sharp absorbing or reflecting boundaries are provided in the Supplementary Material. Lastly, we restrict $\epsilon \leq 0.5$ to reflect the

assumption that host-parasitoid populations exhibit limited dispersal, consistent with empirical observations in many ecological systems.

2.4. Results

Figure 2.3 shows the mean host density at steady state across different levels of heterogeneity (η) for both absorbing and reflecting landscapes. These values represent a combined spatial average (across all habitable patches) and temporal average (over the final 1000 generations), further averaged across 1920 independent landscape realizations. Error bars in Figure 2.3 represent 95% confidence intervals, computed using bootstrap resampling over the 1920 landscape realizations. Based on these results, we identify three distinct qualitative dynamical regimes:

(1) **Phase 1 (low migration, $\epsilon < 0.2$)**: In this regime, migration between patches is minimal, resulting in weak coupling across the landscape. As a result, patches oscillate largely independently of one another. This is supported by the low to moderate temporal correlation between neighboring patches observed in Figure 2.4. Because host outbreaks are asynchronous in space, the mean host density remains low. Heatmaps in Figure 2.5a and 2.5d illustrate this spatially disordered pattern for a landscape with $\eta = 0$ and $\eta = 0.1$ respectively. The presence of a small number of uninhabitable patches ($\eta > 0$) has little to no impact on the overall dynamics or mean host density in this phase.

(2) **Phase 2 (intermediate migration, $0.2 < \epsilon < 0.4$)**: With moderate migration, the coupling between the patches strengthens and the oscillations in the landscape become increasingly synchronized. This is reflected in the high temporal correlation between adjacent patches (Figure 2.4). Synchronous local outbreaks result in large-scale host population surges across the landscape (Figure 2.5b and 2.5e), leading to a substantial increase in mean host density. As in Phase 1, the presence of a small number of uninhabitable patches has minimal effect on the overall steady state or mean host density (Figure 2.3).

(3) **Phase 3 (high migration, $\epsilon > 0.4$)**: In the absence of heterogeneity ($\eta = 0$), the system continues to behave similarly to Phase 2, with slightly higher mean host densities due to increase in coupling. However, in heterogeneous landscapes ($\eta > 0$), we observe a sharp drop in the mean host density (Figure 2.3). This shift is accompanied by a qualitative change in spatial dynamics: instead of synchronous outbreaks, we observe the emergence

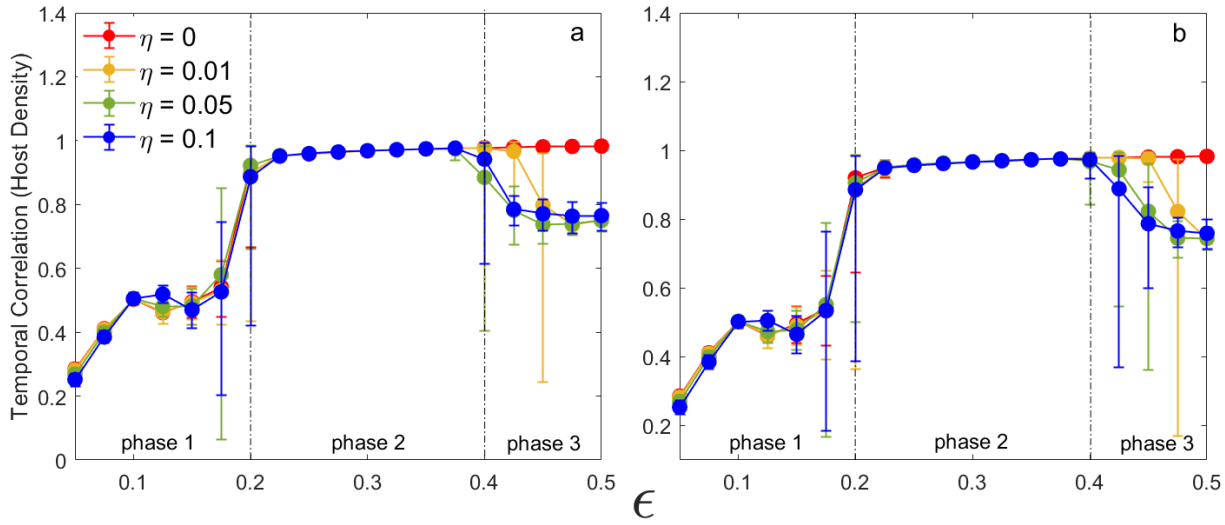

FIGURE 2.4. Mean steady-state temporal correlation between host densities in adjacent habitat patches as a function of migration fraction (ϵ) for (a) absorbing and (b) reflecting boundary conditions, across varying levels of landscape heterogeneity (η). The temporal correlation was calculated over the last 1000 generations of the simulation, averaged over 100 habitat pairs randomly selected across the landscape lattice. Upper and lower error bars in the mean correlation were calculated using Fisher's index. Vertical dashed lines indicate approximate locations of qualitative shifts in the system dynamics, dividing the dynamics into three distinct phases. At low migration (Phase 1), the adjacent patches show weak positive correlation, leading to asynchronous outbreaks in patches across the landscape, as shown in both Figure 2.3 and 2.5. Intermediate migration rates (Phase 2) show strong positive correlation between the host densities in adjacent patches. This leads to spatially synchronized host outbreaks and substantially increased host densities across the lattice as shown in Figure 2.5. At higher migration (Phase 3), mean temporal correlations remain high in homogeneous landscapes ($\eta = 0$), whereas heterogeneous landscapes exhibit a dip in temporal correlation to moderate positive values. This highlights how even small landscape heterogeneities can profoundly impact spatial synchronization and host-parasitoid dynamics, particularly at higher migration rates.

of persistent wave-like structures that propagate through the lattice (Figure 2.5f). This is a marked departure from the landscape-spanning outbreaks seen in Phase 2 (Figure 2.5e), and it leads to reduced host abundance at steady state.

We also observe a minor increase in mean host density in Phase 3 for heterogeneous landscapes when the behavior near uninhabitable patches is reflective (Figure 2.3b), compared to their absorbing counterparts (Figure 2.3a). In absorbing landscapes, migration into uninhabitable patches results in mortality, leading to slightly lower host densities at high migration rates. In contrast, when populations avoid uninhabitable patches (reflective case), this mortality is avoided, yielding

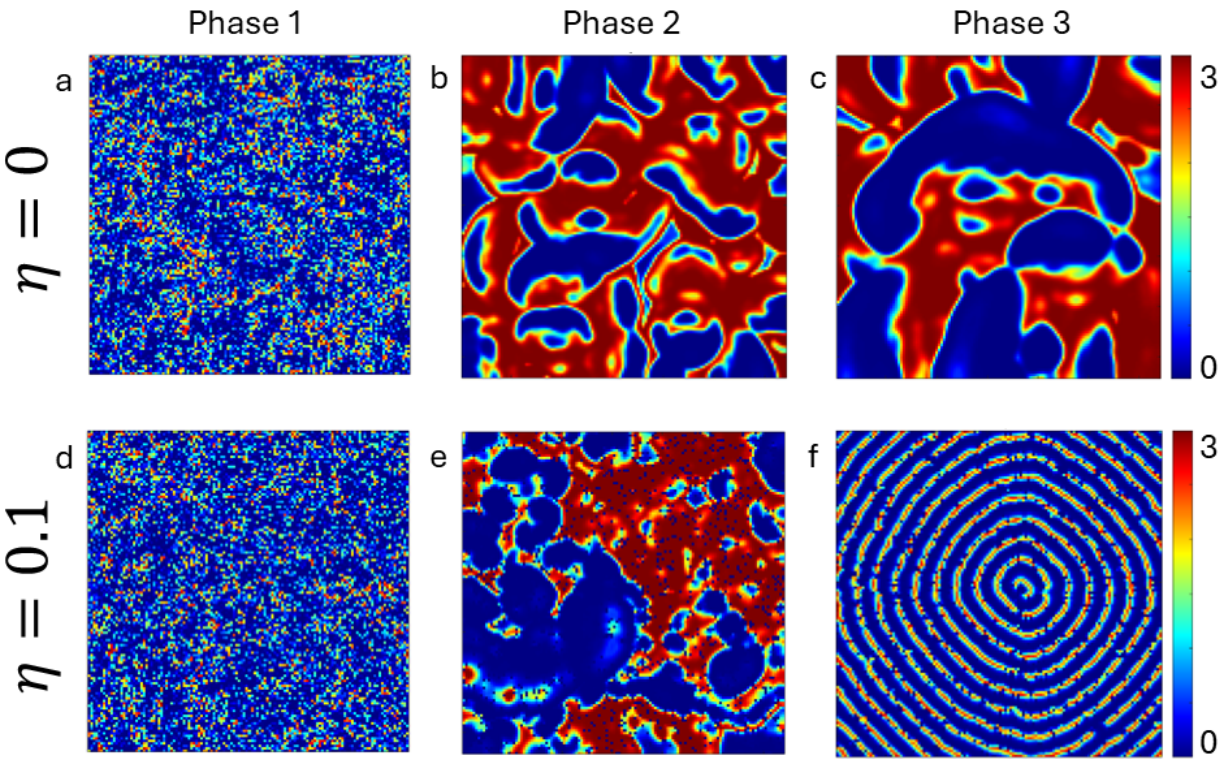

FIGURE 2.5. Heatmaps illustrating steady-state host densities across a spatial lattice for landscapes without heterogeneity ($\eta = 0$, top row: panels (a–c)) and with heterogeneity ($\eta = 0.1$, bottom row: panels (d–f)) for three migration fractions (ϵ), corresponding to qualitatively different dynamical regimes (Phases 1–3). At low migration ($\epsilon = 0.05$, Phase 1, panels (a,d)), host densities appear spatially random with no distinct large-scale patterns, indicating asynchronous local dynamics. At intermediate migration ($\epsilon = 0.3$, Phase 2, panels (b,e)), coherent and synchronized host population outbreaks emerge, forming extensive interconnected high-density regions (red), interspersed with regions of population collapse (blue). Small-scale heterogeneities can be observed in panel (e) as small dark spots interrupting these outbreaks. At higher migration ($\epsilon = 0.45$, Phase 3, panels (c,f)), the presence of uninhabitable patches dramatically alters dynamics. In panel (c) (homogeneous case), large synchronized host outbreaks persist, similar to Phase 2, whereas in panel (f) (heterogeneous case) we see persistent spiral wavefronts radiating outward from localized source-like regions. These persistent wavefronts suppress large-scale host outbreaks, significantly reducing mean host density, as quantified in Figure 2.3.

marginally higher densities.

Interestingly, in the absence of heterogeneity ($\eta = 0$), we find no significant difference in host density between absorbing and reflecting boundary conditions. This suggests that for our system size ($L = 128$), boundary effects are negligible. A heuristic explanation can be derived by comparing

the relative contributions of boundaries and interior habitat. The total number of boundary sites scales with $B = 4L$, while the number of habitable patches is $H = (1-\eta)L^2$. The effect of boundaries on mean host density therefore scales as $\frac{B}{H} = \frac{4}{(1-\eta)L} \approx \frac{1}{L}$ for small η, and diminishes with increasing system size. In contrast, the effect of uninhabitable patches scales as $\frac{\eta L^2}{(1-\eta)L^2} = \frac{\eta}{1-\eta}$, which is independent of L. This implies that while the influence of boundaries decreases in larger systems, the effect of internal heterogeneity persists. We further support this conclusion with results from homogeneous landscapes under absorbing, periodic, and reflective boundaries, provided in the Supplementary Material.

To quantify the degree of synchrony between neighboring patches, we computed the Pearson correlation coefficient between host density time series from 100 randomly selected adjacent habitat patch pairs across the lattice. Correlations were calculated over the final 1000 generations at steady state, averaged first over the 100 habitat patch pairs, and then across 1920 independent landscape realizations. To account for skewed distributions and to compute statistically robust error bars, we applied Fisher's Z-transformation to the correlation values before calculating 95% confidence intervals. The error bars in Figure 2.4 represent these intervals mapped back into correlation space. Figure 2.5 shows representative steady-state heatmaps for both homogeneous ($\eta = 0$) and heterogeneous ($\eta = 0.1$) landscapes under reflecting conditions. We focus on reflecting cases for visualization to isolate the effects of heterogeneity and migration, without the confounding influence of mortality due to migration present under absorbing conditions. In homogeneous landscapes, we observe two distinct spatial regimes: (1) an asynchronous, spatially disordered pattern at low migration (Figure 2.5a), and (2) a synchronized landscape-wide outbreak cycle at intermediate to high migration (Figures 2.5b, c). However, in heterogeneous landscapes, a third qualitative regime emerges at high migration (Phase 3), characterized by persistent traveling spiral waves of host density that radiate outward and dominate the spatial dynamics (Figure 2.5f).

Together with host density trends (Figure 2.3) and temporal correlation patterns (Figure 2.4), these spatial patterns illustrate how increasing migration promotes local synchrony, and under heterogeneous conditions, leads to qualitatively distinct spatial structure. To understand the origin of

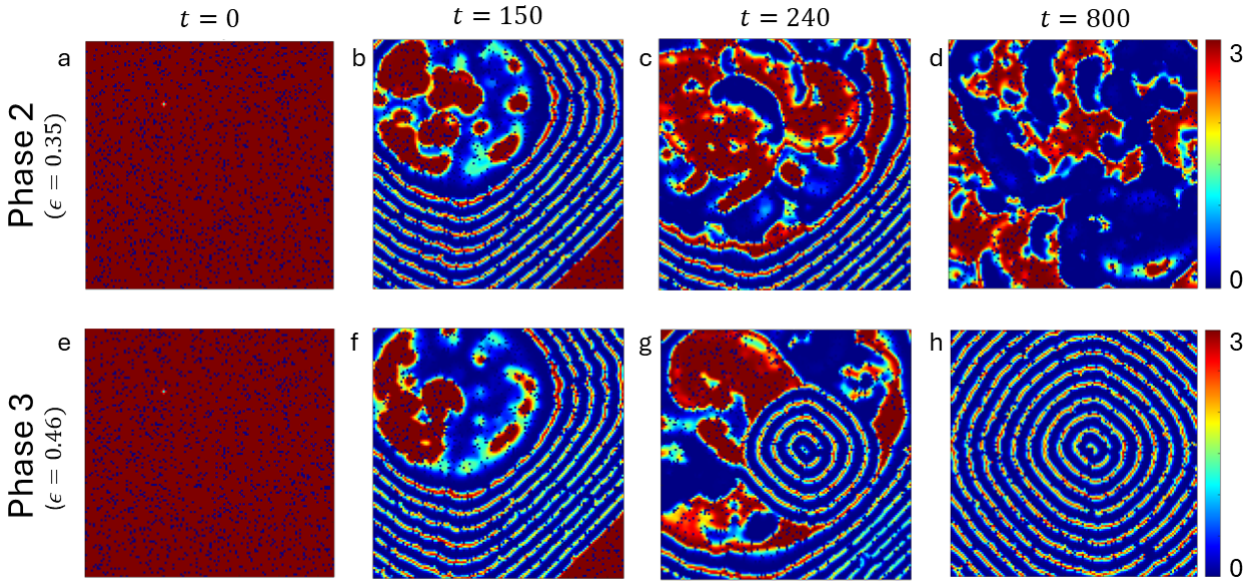

FIGURE 2.6. Heatmaps illustrating the temporal development of host densities from initial transient dynamics toward steady state in a heterogeneous landscape ($\eta = 0.1$) under reflecting boundary conditions. Panels (a,e) depict the initial condition at $t = 0$, with host populations initialized at carrying capacity throughout all habitable patches (red), and parasitoids introduced at a randomly selected habitable patch (visible as a yellow dot). Panels (b–d) correspond to intermediate migration ($\epsilon = 0.35$, Phase 2), showing initial parasitoid-driven wave propagation (panel b), which colonizes the lattice (the dark blue wavefronts indicate host depletion due to parasitism). Eventually, steady-state dynamics characterized by large synchronized host-density clusters form and dissipate cyclically (panels c,d). Panels (f–h) illustrate dynamics at high migration ($\epsilon = 0.46$, Phase 3), where after initial wave propagation (panel f), distinct and persistent traveling spiral wavefronts of host density emerge (panels g,h). These waves originate from localized sources and suppress large-scale synchronized host clusters. The spiral waves arise due to a spatial interplay between host refugia created indirectly by uninhabitable patches, parasitoid-driven host depletion, and rapid host recolonization enabled by high migration. Such persistent wave patterns significantly reduce mean host densities in highly migratory scenarios.

the spiral waves observed in Phase 3, we examined the early time series of the simulation (Figure 2.6). Initially, parasitoids introduced at a single patch spread outward in waves, depleting host populations across the lattice (Figures 2.6a,f). These transient wavefronts result from symmetric dispersal combined with local outbreak-crash-buildup cycles (Figure 2.1a). At intermediate migration rates (Phase 2), large-scale host outbreaks eventually span the lattice, forming a synchronized steady state (Figures 2.6c,d). In contrast, at higher migration (Phase 3), spiral waves originate

near clusters of uninhabitable patches (Figure 2.6g). These uninhabitable patches act as spatial refuges by delaying parasitoid arrival, allowing the host-dominated patches to recolonize adjacent areas depleted by previous parasitoid attacks. This interplay between this spatial refuge effect, local host-parasitoid oscillations, and rapid recolonization - amplified by high migration—creates rotating wavefronts that propagate outward. Over time, these spiral waves outcompete and suppress other outbreak patterns, establishing a steady-state dominated by persistent traveling waves (Figure 2.6h).

2.5. Discussion

Understanding how spatial structure and dispersal interact to shape population dynamics has been a central theme in theoretical ecology. Prior studies have highlighted the stabilizing and destabilizing effects of spatial coupling in predator-prey and host-parasitoid systems [24], the emergence of complex dynamics and chaos in spatially extended systems [33, 58], and the role of synchrony in driving large-scale insect outbreaks [19, 87]. Metapopulation models have been widely used to investigate these questions, offering insight into how dispersal affects extinction risk, recolonization, and regional persistence. However, many of these models adopt simplifying assumptions, such as spatial homogeneity and periodic boundaries, which may limit their ability to capture the full range of spatial dynamics observed in real ecosystems. Dynamical systems are known to be sensitive to underlying spatial structure, and even minor deviations from homogeneity can yield qualitatively different behaviors. Neutral landscape models have demonstrated that small-scale structural variation in habitat layout - often interpreted as forms of habitat loss or fragmentation - can significantly influence population persistence, spatial synchrony, and species interactions [129, 134]. Motivated by these insights, we ask whether the key relationships inferred from these ideal metapopulation models - particularly those linking migration rate and host density - remain robust when small amounts of spatial heterogeneity (habitat losses) are introduced. Specifically, we examine how the presence of small but randomly distributed uninhabitable patches alters mean host densities and emergent spatial patterns in host-parasitoid systems.

One of the novel result of our model is the significant decline in mean host density at high migration rates (Figure 2.3), illustrating how small-scale habitat loss, modeled here as spatial heterogeneity,

can shift core ecological relationships. Previous studies have attributed such declines in host density at high migration rates to migration-induced mortality, particularly in systems with absorbing boundaries or dispersal into unsuitable habitat [67]. More recent studies has since provided a more nuanced view: for example, when parasitoids are more mobile and experience higher mortality, top-down control weakens and host densities can rise [72]. In contrast, a higher host dispersal mortality leads to lower host densities. In addition, [108] and [68] showed that habitat loss can benefit herbivores when parasitoids are more mobile, contradicting earlier models that excluded mortality and predicted the opposite.

In contrast to these studies, our model keeps migration rates identical for both hosts and parasitoids, eliminating differential dispersal as a driver of population imbalance. Moreover, we observe similar declines in host density even under reflective boundary conditions, where migration-induced mortality is explicitly excluded. This indicates that the reduction in host density at high migration is not a consequence of direct loss, but instead emerges from structural changes in spatial dynamics introduced by landscape heterogeneity. Uninhabitable patches - analogous to fine-grained habitat loss - alter the pathways of movement and create localized spatial refuges that delay parasitoid spread, allowing hosts to recolonize and form rotating wavefronts that reshape outbreak dynamics. This mechanism highlights a novel pathway by which spatial structure - not mortality - can regulate host densities, even in the absence of asymmetric dispersal. Our findings extend the literature on the relationships between migration and host suppression by demonstrating that it can arise purely from the interaction between dispersal and spatial heterogeneity in structurally simple but ecologically realistic metapopulation systems.

Our results reveal three distinct spatial regimes: asynchronous local oscillations at low migration, synchronized landscape-wide outbreaks at intermediate migration, and a novel spiral wave regime at high migration in heterogeneous landscapes. The emergence of these spiral waves - absent in homogeneous models - marks a key qualitative shift in system behavior driven by the interaction of migration and spatial heterogeneity. Unlike classical spiral wave models that rely on reaction-diffusion frameworks or explicit oscillatory coupling [110, 111, 124], our model demonstrates that

simple host-parasitoid dynamics combined with random uninhabitable patches in a discrete lattice can give rise to persistent wavefronts. This complements findings in [33, 111] and [19], but highlights a distinct mechanism tied to heterogeneity rather than deterministic cycling or external forcing.

The spiral waves we observe originate near uninhabitable patches, which act as spatial refuges where host populations can temporarily escape parasitoid suppression. These patches delay the arrival of parasitoids, allowing host densities to rebound and recolonize adjacent areas, especially under high migration. This dynamic interplay creates rotating wavefronts that propagate outward, suppressing other outbreak regions and establishing a new steady-state dominated by traveling waves. These findings parallel the insights of [58, 111], who showed that local interactions and spatial structure can create self-organizing patterns, but our results emphasize how even minimal heterogeneity can catalyze such structure in discrete systems.

Temporal correlation analysis further supports our classification of spatial regimes. At low migration, adjacent patches show weak correlation due to asynchronous dynamics. As migration increases, correlation strengthens, supporting synchronized outbreaks. However, in heterogeneous landscapes at high migration, correlation decreases again, indicating a shift from global synchrony to localized traveling waves. This mirrors earlier work on second-order spatial correlations in host-parasitoid systems [33], but provides a new lens for interpreting transitions between synchrony and patterning.

Our study also reinforces and builds upon themes from the literature on neutral landscape models (NLMs). As emphasized by [129] and critiqued in [134], idealized landscapes can obscure the role of spatial structure in ecological dynamics. By modifying a standard metapopulation model with minimal heterogeneity - interpretable as small-scale habitat loss, we demonstrate that core ecological insights - such as the relationship between dispersal and population density - are sensitive to spatial assumptions. This suggests that NLMs must be used with caution when interpreting migration-synchrony relationships.

Importantly, we find that absorbing and reflecting behavior near heterogeneities can yield similar spatial outcomes at intermediate migration rates, cautioning against inferring individual movement rules solely from landscape-scale patterns. Two different behavioral assumptions can produce comparable outbreak synchrony, a finding with direct implications for empirical inference in fragmented landscapes [87].

Our results raise important questions about the link between local structure and global outcomes—a central challenge in spatial ecology. While we focused on low levels of random heterogeneity ($\eta \leq 0.1$), future work could explore how different spatial configurations (e.g., clumped, fractal, or interior boundaries) influence wave formation, persistence, and host suppression. These spatial heterogeneities may stem from ecological processes such as disturbance, succession, or anthropogenic habitat loss. Another direction is to investigate local variation in patch connectivity. In our lattice, most patches have four neighbors, with the exeption of very few patches adjacent to uninhabitable areas - reflecting minor habitat loss. Higher levels of heterogeneity, achieved by increasing η, may lead to habitat fragmentation where core outbreak dynamics collapse. Habitat fragmentation is a central theme in neutral landscape theory and has often been explored through the lens of percolation theory, which examines how connectivity is lost as habitat availability falls below critical thresholds [134]. Understanding how patch-scale structure and connectivity scales up to affect landscape-level synchrony remains a crucial step toward integrating individual-based mechanisms with broader ecological predictions [19].

Finally, modifying the dispersal structure - e.g., through a local dispersal kernel rather than strict nearest-neighbor migration - could reveal how wave structures respond to broader spatial coupling. Such extensions could improve the applicability of discrete models to real-world systems, where dispersal is rarely symmetric or strictly local.

Our study shows that even minimal heterogeneity can fundamentally alter host-parasitoid metapopulation dynamics, introducing new spatial regimes that are not observed in homogeneous systems. The emergence of spiral waves from simple heterogeneity, the reduction in host density independent of migration-induced mortality, and the context-dependent role of boundary behavior underscore

the importance of spatial structure in ecological modeling. These results highlight the need to move beyond idealized assumptions in metapopulation theory and provide a framework for understanding how local interactions and spatial context jointly shape large-scale ecological patterns.

2.6. Code availability

All codes used for this project can be found here -https://doi.org/10.5281/zenodo.15302303.

2.7. Acknowledgements

This work was funded by NSF grants DMS-1817124 and 1840221 and 2325076.

CHAPTER 3

Assessing Impacts of Bycatch Policies and Fishers' Heterogeneous Information on Food Webs and Fishery Sustainability

Abstract

Ecosystem based fisheries management (EBFM) has emerged as a promising framework for understanding and managing the long-term interactions between fisheries and the larger marine ecosystems in which they are nested. However, a successful implementation of EBFM has been elusive because we still lack a comprehensive understanding of the network of interacting species in marine ecosystems (the food web) and the dynamic relationship between the food web and the humans who harvest those ecosystems. Here, we advance such understanding by developing a network framework that integrates the complexity of food webs with the economic dynamics of different management policies. Specifically, we generate hundreds of different food web models with 20-30 species each harvested by five different fishers extracting the biomass of a target and a bycatch species, subject to two different management scenarios and exhibiting different information in terms of avoiding bycatch when harvesting the target species. We assess the different ecological and economic consequences of these policy alternatives as species extinctions and profit from sustaining the fishery. We present the results of different policies relative to a benchmark open access scenario where there are no management policies in place. The framework of our network model would allow policymakers to evaluate different management approaches, without compromising on the ecological complexities of a fishery.

3.1. Introduction

Fisheries across the world remain vital as ever as they serve food, economy and livelihood to communities, locally and globally [9, 53, 116]. Fish and fish products are one of the most traded goods in the world [7, 10, 16, 38, 117]. Continual pursuit of profits that come from selling fishing products has led to fishing practices that threaten marine biodiversity, fishers' safety, and food

security [8, 39, 41, 81, 104]. Current fishery management practices have had partial successes in rebuilding fish stocks in collapsed fisheries and towards maintaining long term sustainability of fisheries [14, 64, 65, 89]. However, effective fishery management can be hindered by a host of factors, including failure to incorporate scientific knowledge [98], lack of compliance with fishery regulation [12], lack of ecological, catch or stock assessment data [43], and failure to account fully for ecosystem interactions [13, 136]. In this paper, we focus on the last factor. That is, incorporating into management an understanding of the dynamic interaction of species throughout the marine food web, including impacts from human harvest.

Considering the food web to which the harvested species belong is a core element of Ecosystem-Based Fisheries Management (EBFM), which has emerged over the past 2 decades as a promising complement to stock-centric, single species management [37,70,89,90,104]. EBFM recognizes that effective management should not only focus on individual commercial species but also consider the broader ecosystem context, and seek a balance between ecological resilience and economic viability [25, 42, 88, 104]. EBFM focuses, for example, on reducing excessive levels of bycatch associated with fishing [5, 63, 106], as these commercially unwanted species play significant role in ecosystem functioning [88, 104]. However, implementing EBFM is challenging because it not only requires knowledge of the dynamics of the commercial species but also that of the network of interactions between the commercial species and the other species in the ecosystem [37, 54]. This ecological network determines how species affect each other and, therefore, how each species is affected directly or indirectly (e.g., via changes in abundance of its prey or predators) by fisheries [36, 47, 71, 91, 113, 122, 127]. Likewise, the ecological network may determine that a fish stock declines despite policy prohibiting its harvest if the fishery, for example, is extracting its prey. The challenge lies in understanding these complex dynamics and predicting how various changes, such as policy interventions, might impact ecological and economic outputs. While regulators in the U.S. and elsewhere are being pressed to incorporate EBFM, given the complexity of implementation, development and application of this framework is still "evolutionary rather than revolutionary" [90]. While traditional single-species models have moderate success in reducing overfishing of commercially important target species and incidental catch of endangered species, they fall short in capturing the complex dynamics that emerge from the ecological network [28, 71, 127]. To address this, we turn to ecological network theory (e.g., [47, 91, 122]). Ecological networks allow us to model

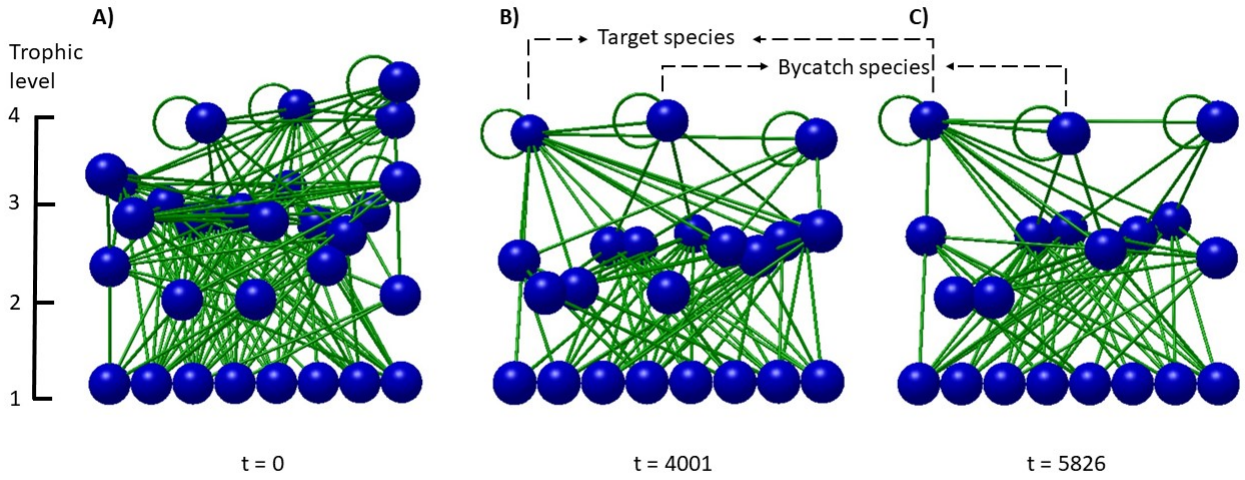

FIGURE 3.1. An example of the temporal change of a food web network from (A) initialization, to (B) the start of fishing, to (C) after five years of fishing. Trophic species are represented by nodes, trophic interactions (who eats whom) as links, and the vertical axis represents the trophic level of species. The (A) initial network is generated using the niche model. The Allometric Trophic Network (ATN) model is then run for 4000 daily time steps with the biomass of each species changing over time according to Equations 1 and 2 (see Methods). Subsequently, a target species and bycatch species are selected, and fishing occurs for an additional 5 years (1826 time steps).

species as nodes and their interactions as links, as well as, model the population dynamics of every species in the network using ordinary differential equations, which is affected by its interactions with other species in the network. Specifically, we use the well-known and widely-used Allometric Trophic Network (ATN) framework [17, 26, 36, 45, 47, 81, 91, 122] to model the dynamics of marine food webs, which is an extension of the bioenergetic model by Yodzis and Innes [135] to multi-species systems. Allometric scaling in this framework provides a biologically informed way to parameterize trophic interactions and ecological processes based on metabolic theory and life history traits (e.g., trophic level and vertebrate/invertebrate) [135]. Therefore, this framework is very useful for developing general understanding on food web dynamics and on how they generally respond to anthropogenic changes including disturbance caused by fisheries (e.g., [36, 47, 81, 122]). This general understanding of food web dynamics differs from the more system-specific understanding produced by approaches like Ecopath with Ecosim, for which system specific parameters need to be determined extensively (e.g., [103, 105]).

Here, we seek to advance the theoretical framework of EBFM by introducing three bioeconomic factors that have not been considered in ecological networks before. These factors are: 1) unintentional bycatch, defined as species caught incidentally during fishing operations, 2) heterogeneity in fishing success (based on their access to information) among individual fishers, measured in their ability to catch commercially important target species and avoid unwanted bycatch species, and 3) different fishery management policies to achieve long term ecological and economic sustainability of the fishery. This approach allows us to investigate the complex interplay between the species in the ecological network, their interaction with heterogeneous fishers, and intervention by management policies to attain long term sustainability. We achieve this by incorporating fishers with different levels of fishing success as additional nodes into the ecological network, connected exclusively to target and bycatch species, and simulating different fishery policies that close the fishing season for the year when the target quota and/or the bycatch quota are met. Indeed, our model advances from previous ecological network models (i.e., [47]) by successfully replicating average active fishing seasons, which typically ranges from a few weeks to few months a year [6, 62, 112].

The three bio-economic factors we introduced in our network model are well-studied in the bio-economic literature but only for a handful of species in that ecosystem [15, 21, 30, 77]. Thus, our work contributes to the bio-economic literature by considering the entire ecological network to which the target and bycatch species belong. We focus on management policies that play a crucial role in shaping the dynamics of fisheries but whose consequences can be far-reaching and sometimes unexpected because of the complex dynamics caused by the ecological network [76,101,136]. Specifically, we evaluate the effects of various management policies on both ecological and economic aspects and investigates trade-offs between conserving species, sustaining yields, and promoting economic stability. Finally, we present new insights into the potential for sustainable fishing practices without compromising substantial economic profits and the employment fisheries provide.

3.2. Methods

Experimental setup and policy implementation. We first generated trophic networks (food webs) using the niche model [131] (see next sub-section). Food webs generated using the niche model replicate observed empirical patterns (particularly in aquatic ecosystems) in features

like distribution of trophic species across different trophic levels and mean trophic chain length, among others [131]. Each species in the food web was then assigned an initial biomass using a uniform distribution, $U\epsilon(0,1)$. Subsequently, the ATN framework (detailed in the "Ecological and economic dynamics" section) characterized by Eqs. 1 and 2, was applied to simulate each food web across a sequence of 4000 time steps, without any fishing. This preliminary period without fishing serves to dampen the potential impact of transient dynamics on the subsequent outcomes of fishery treatments.

Following this initial fishing-free interval, fishing is introduced only in those food webs which meet the following criteria: i) is connected (i.e., no isolated components), ii) all consumers are linked to at least one basal species (primary producers) through trophic interactions, iii) has at least 20 species, and iv) has at least one fish species. This treatment led to 400 distinct food webs which was subjected to an additional 1825 time steps, equivalent to 5 years.

At the start of fishing, a target species and a bycatch species were selected among consumer species with trophic level equal or above 2 (to avoid choosing a producer species). The target species was selected randomly at the end of the fishing free interval (i.e., t = 4000). Bycatch was either selected randomly or as the consumer species which had the lowest biomass at the end of the fishing free interval (henceforth referred as vulnerable bycatch species). Each day, the biomass of species change based on Eqs. 1 and 2., after which two conditions are evaluated: 1) Is the fishery (given current target species biomass levels) profitable for at least one fisher? 2) Do the biomasses of species trigger constraints given by the policy (detailed in section "Policies"), if any, in place? Once either of the two conditions fail, the fishery is shut down (all fishers efforts are set to 0) for the remainder of the year. In the following year, if the biomasses of the species meet the two conditions, the fishery is open and the cycle continues. The annual dynamics mimic annual fishery closures which are features of real world fisheries for biomass of target species to recover [31, 32]. An example of time series from our model is shown in Figure 3.2.

The dynamics of the food webs were run for each policy scenario, for all target-bycatch combinations possible in each food web. We calculated ecological (see Figure 3.3) and economic (see Figure 3.4) metrics as averages over all possible target-bycatch combinations and over all networks. All simulations were run in MATLAB 2021a using the solver ode45 for numerical integration with relative and absolute error tolerances both equal to 10^{-8}.

Network/food web structure. The network structure outlines the connections between fishers, prey, and predators. Initially, each niche-model-generated food web consisted of 30 trophic species, where trophic species (S) represent groups of individuals sharing the same resources (i.e., prey species or primary producers such as algae or phytoplankton) and consumers (i.e., predator or herbivore species consuming producers). These webs had connectance of 0.125 - 0.175, where connectance (C) indicates the proportion of realized trophic links $\left(\frac{L}{S^2}\right)$, with L representing realized links. Each of the 30 trophic species is assigned a niche value along a single trait axis (interpreted here as body size, see next sub-section). Species i preys on species j if j's niche value falls within i's feeding range, allowing for potential consumption of species with higher niche values, which accounts for cannibalism. The feeding range of the lowest niche species is set at 0, which imposes that at least one primary producer is present. Niche values for the 30 trophic species are assigned iteratively, ensuring three criteria are met: i) network connectivity (i.e., there are no isolated nodes/components), ii) linking each consumer species to a primary producer via a trophic chain, and iii) achieving connectance within the predetermined range of 0.125 - 0.175. Fish species are identified among consumer species using a Bernoulli trial (P = 0.6), while the remaining species are treated as invertebrates.

Ecological and economic dynamics. The biomass dynamics of each trophic species within a generated food web is determined by an ordinary differential equation with parameters scaled allometrically by the Allometric Trophic Network (ATN) model. The ATN model has enriched our understanding of food web dynamics by offering flexible approaches to model the biomass dynamics of dozens to hundreds of interacting species, while retaining tractability [17,26,36,47,81,91,122]. This model describes the rate of biomass change ($\frac{dB_i}{dt}$) of species i depending on whether the trophic species is a primary producer (Eq. 1) or a consumer (Eq. 2) as follows:

$$\overbrace{\frac{dB_i}{dt}}^{\text{Rate of change in producer biomass}} = \overbrace{r_i\Big(1-\frac{\sum_{k\,\epsilon\,\text{producers}} B_k}{K}\Big)B_i}^{\text{Net primary production}} - \overbrace{\sum_{j\,\epsilon\,\text{predators}} x_j \frac{y_j}{e_{ji}} F_{ji} B_j}^{\text{Loss by herbivory}}, \tag{3.1}$$

$$\overbrace{\frac{dB_i}{dt}}^{\text{Rate of change in consumer biomass}} = \overbrace{f_a \sum_{j\,\epsilon\,\text{prey}} x_i y_j F_{ij} B_i}^{\text{Gains by consumption}} - \overbrace{f_m x_i B_i}^{\text{Maintenance loss}} - \overbrace{\sum_{j\,\epsilon\,\text{predators}} x_j \frac{y_j}{e_{ji}} F_{ji} B_j}^{\text{Loss by predation}} - \overbrace{H(B_i, E_{ki})}^{\text{Harvest loss}}. \tag{3.2}$$

Time-varying variables and constants are indicated by upper and lower case fonts, respectively (values and definitions provided in Table 1). For variables with two indices (e.g., e and F) the first index represents a consumer species (predator or herbivore) and the second represents its resource species (its prey or primary producer). r_i is the growth rate of producer species i. Fractions f_a and f_m signify the assimilated carbon used in production and maintenance respiration, respectively, which allows for realistic biomass transfers across trophic levels ([79]). x_i is metabolic rate (rate at which an organism expends energy in physiological processes), defined by $x_i = \frac{a_x}{a_r}(Z^{T_i-1})^{-0.25})$, where a_x is the allometric constant that relates the metabolic rates of consumers to their body size, a_r the allometric constant that relates the reproductive rates of producers to their body size, Z the body size ratio, and T_i, the trophic level [27, 46, 135]. y_i represents maximum consumption rate of species i, and e_{ji} represents the efficiency of converting biomass of species i when consumed by species j into its biomass.

Dividing "loss by herbivory (or predation)" by e_{ji} transforms the biomass assimilated by consumer j into biomass lost of its resource i (see [135]). F_{ij} is the consumer i's functional response on j (i.e., per-capita consumption rate). Following all prior studies using the ATN framework (e.g., [17, 26, 47, 81, 91, 122]), we used what it has been called a "type II.2" (or weak Holling-type III) functional response [132] which has a stabilizing effect on food web dynamics [52, 132] and it is supported by general empirical understanding of consumer-resource interactions because this response can capture some of the well-known consumer preference for more abundant resources. This functional response is given by:

$$F_{ij} = \frac{\omega_{ij} B_j^h}{B_{0,j}^h + \sum_{k\ \epsilon\ \text{prey}} \omega_{ik} B_k^h}. \tag{3.3}$$

$B_{0,j}^h$ is i's half-saturation biomass for its resource j. ω_{ij} is i's preference for its resource j, calculated as the reciprocal of the total number of i's resource species and is re-calculated as resource species become extinct. h is the hill coefficient, which sets the sensitivity of the functional response to resource's biomass.

The timescale of the dynamics in each food web is established following Glaum et al. ([47]), where one model time step corresponds to one real-time day. This timescale results from setting the mass-specific growth rate of all producers to $r_i = 1$. This rate then normalizes metabolic (x_i) and maximum consumption (y_i) rates as in most studies using the ATN model (e.g., [17, 26, 47,

81, 91, 122]). We use an extinction threshold of $B_{ext} = 10^{-6}$, below which we assume a species as locally extinct.

Ecological Parameters	Description	Value (units)	Source
r_i	Growth rate of species i	1 (time^{-1})	[47]
K	Carrying capacity	1 ($\frac{\mu gC}{L}$)	[26]
e_{ji}	Assimilation efficiency of predator j given that prey consumed i is a carnivore or herbivore	Carnivore: 0.85, herbivore: 0.45	[26]
a_r	Allometric constant relating reproductive rates of producers to their body size	Variable	[26]
a_x	Allometric constant relating metabolic rates of consumers to their body size	Variable	[26]
a_x/a_r	Allometric constant	Invertebrate: 0.314, fish: 0.88 (time^{-1})	[26]
y_i	Maximum consumption rate of species i relative to its metabolic rate	Invertebrate: 8, fish: 4	[26]
Z	Body size ratio	100	[26]
B_0	Half saturation biomass	0.2 ($\frac{\mu gC}{L}$)	Assumed
h	Hill coefficient	1.2	[130]
B_{ext}	Extinction threshold biomass (used in simulations)	10^{-6} ($\frac{\mu gC}{L}$)	[109]
ω_{ij}	Preference of species i for species j	Variable	
F_{ij}	Functional response of predator species i for prey species j	Variable	
f_m	Factor for maintenance respiration	0.4	Assumed
f_a	Fraction of assimilated carbon used for production	0.4	[20]
x_i	Metabolic rate of species i	Variable (time^{-1})	
Economic Parameters	**Description**	**Value**	**Source**
$E_{\max}$	Maximum effort	1	Assumed
q_{target}	Catchability coefficient for target species	0.002	Assumed
q_{bycatch}	Catchability coefficient for bycatch species	0.002	Assumed
ψ	Threshold for profitable fishery	0.25	Assumed
p	Market price	1	Assumed

TABLE 3.1. Parameter definitions, values and sources. Units are indicated for parameters, except when they are unitless.

Biomass loss due to harvesting ($H(B_i, E_{ki})$ in Eq. 2) is dependent on the biomass of the harvested species i (B_i) and the fishing effort of fisher k on species i (E_{ki}) as follows:

$$H(B_i, E_{ki}) = \begin{cases} \sum_{k \,\epsilon\, \textbf{fishers}} \gamma_k E_{ki} q_i B_i, & \text{if } i \text{ is target} \\ \sum_{k \,\epsilon\, \textbf{fishers}} (1-\gamma_k) E_{ki} q_i B_i, & \text{if } i \text{ is bycatch} \\ 0, & \text{otherwise} \end{cases} \tag{3.4}$$

Effort is a measure of the amount of harvesting resources used in a fishery. Depending on the specific fishery, effort can be a measure of the number of fishing lines, boats, workers, or work hours dedicated to harvesting. Results presented here do not qualitatively depend on the specific details of fishing effort. Each fisher extracts biomass of two species in each food web, one as target and the other as bycatch. The ability of fisher k to allocate their effort towards catching target (and simultaneously avoiding bycatch) is given by γ_k. Fishers differ in their ability to catch target while simultaneously avoiding bycatch. This heterogeneity among fishers could be due to to different levels of skill or access to information on species concentration (as facilitated by information sharing among fishers). We model 5 fishers with $\gamma_k \,\epsilon\, [0.7, 0.75, 0.8, 0.85, 0.9]$. q_i is the catchability of species i.

Within a fishing season, fisher k harvest the biomass of the target species i (B_{target} onward, with $i = \text{target}$) at a constant maximum effort ($E_{\max}$) as long as fishing is profitable. That is, as long as gross profits per unit effort ($\gamma_k p q_{\text{target}} B_{\text{target}}$) are greater than marginal costs of fishing effort (c_0), as follows:

$$E_{k\text{target}} = \begin{cases} E_{\max}, & \text{if } \gamma_k p q_{\text{target}} B_{\text{target}} > c_0 \\ 0, & \text{otherwise} \end{cases} \tag{3.5}$$

Whether it is profitable for fisher k to harvest the target species ($E_{k\text{target}} = E_{\max}$) or not ($E_{k\text{target}} = 0$) depends on their ability to catch the target species (γ_k), market price (p), catchability of target species (q_{target}), the biomass of the target-species at that instant (B_{target}), and the marginal costs of effort (c_0):

$$c_0 = \psi p q_{\text{target}} B_{\text{target}}(t = 0) \tag{3.6}$$

where ψ is a scaling parameter ranging between 0 and 1. Note that, instead of using a fixed value (given by $c_0 = \psi p q_{\text{target}}$), we made the marginal costs of fishing dependent on the biomass of the target species before fishing starts ($B_{\text{target}}(t = 0)$). We chose this set-up because every simulated network is unique in the biomasses of its constituent species, ranging over a few orders of magnitude. Thus, under a fixed value of marginal costs of fishing, some networks have no fishing at all because the costs are higher than the gross profits per unit of fishing effort (when target species has low initial biomass, see Eq. 5), whereas some networks have excess of fishing (when target species has high initial biomass). Therefore, Eq. 6 ensures that there is initial fishing in every network, and allows us to compare various levels of marginal fishing costs across networks.

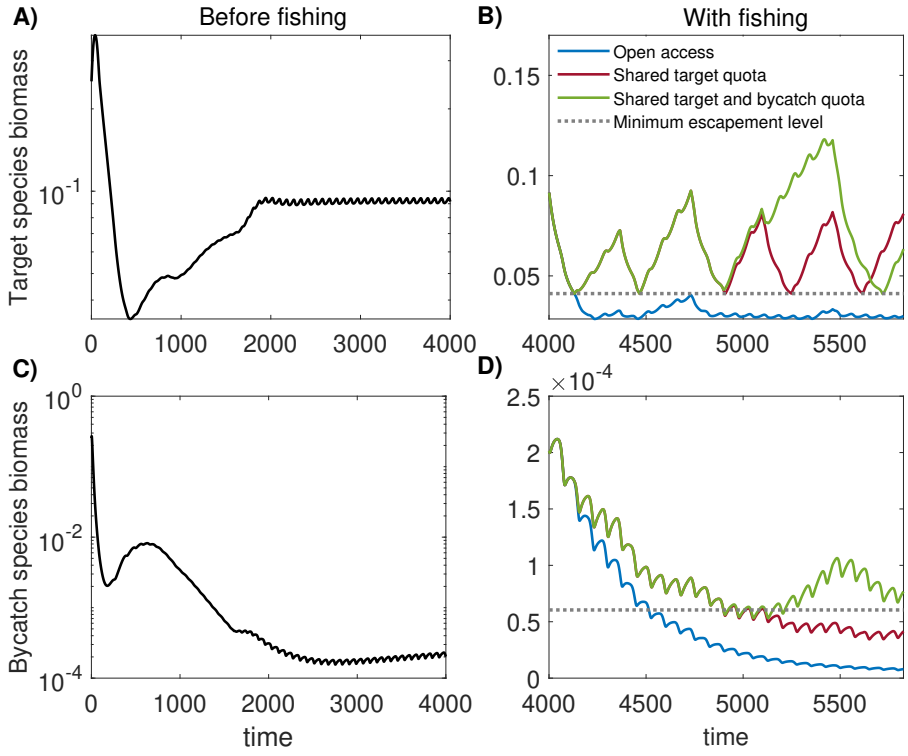

FIGURE 3.2. An example of a simulated time series from a single food web. Before fishing, the biomass of (A) the target species and (C) bycatch species can vary widely before eventually stabilizing (hence the vertical axes are shown in log_{10} scale). Fishing begins under various policies (see legend), with effects on the (B) target species and (D) bycatch species biomass. For policies with a target species quota (allowing fishing down to the minimum escapement level), harvesting periods are evident from declining target species biomass and non-harvesting periods from increasing target biomass. In open access, biomass for both species declines with harvest, which occurs whenever fishing is profitable.

Policies. We incorporated two different policy scenarios and compared our findings with base reference open access, where there is no policy in place:

(1) Open access: Fishing occurs while the fishery is profitable and the target species is not extinct (i.e. biomass of target species is not 0).

(2) Shared target quota: A quota is set equal to the current biomass less a minimum escapement level ($B^{\text{esc}}_{\text{target}}$) for the target species. Fishers harvest until either the quota is exhausted or the profit is negative. Minimum escapement level is the minimum number of fish that are allowed to escape the fishery and spawn to ensure their long term sustainability and avoiding extinctions.

(3) Shared target and bycatch quota: In addition to the shared target quota defined above, a shared quota is similarly set for bycatch species according to a minimum escapement level ($B^{\text{esc}}_{\text{bycatch}}$).

We simulate a range of target and bycatch quotas that follow from a minimum biomass escapement policy, which is specified in each new simulation as a share of the biomass at the onset of fishing: $B^{\text{esc}}_{\text{target}} = \text{esc}_{\text{target}} \cdot B_{\text{target}}(t = \text{onset of fishing})$ and $B^{\text{esc}}_{\text{bycatch}} = \text{esc}_{\text{bycatch}} \cdot B_{\text{bycatch}}(t = \text{onset of fishing})$. To explore a range of policy stringencies, we consider a set of escapement shares $(\text{esc}_{\text{target}}, \text{esc}_{\text{bycatch}})$ given by the vector [0.15, 0.3, 0.45, 0.6]. Figure 3.2B and D shows an example of how different policies manifest in a given simulation, while Figure 3.2A and C shows the transient dynamics in biomass of the target and bycatch species, respectively, until steady state before fishing starts. After fishing begins, the shared target quota allows the target species to recover its biomass substantially during non-harvesting periods (i.e., when the fishery is closed, Fig. 3.2B) and slows down the biomass decline of the bycatch species compared to open access (Fig. 3.2D). Adding the shared bycatch quota allows for recovery of bycatch species whenever it falls to its minimum escapement level (Fig. 3.2D). Thus, as expected, having both target and bycatch quotas results in higher bycatch and target species populations in general.

3.3. Results

We first analyze the effect of different policies on mitigating ecological extinctions of target, bycatch, and all other species in the food web, which we call secondary species. Figure 3.3 shows the average probability of those extinctions for different minimum escapement levels of target ($\text{esc}_{\text{target}}$) and

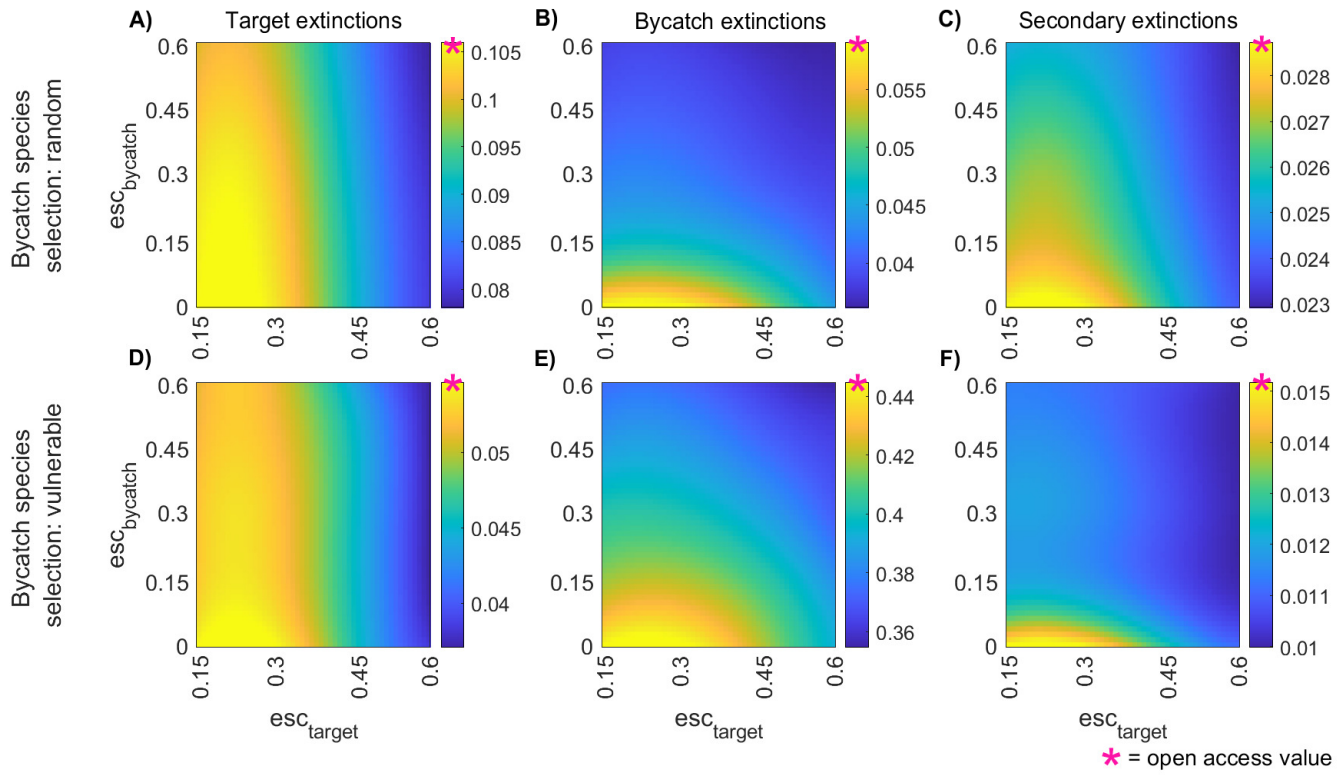

FIGURE 3.3. Extinction probabilities (shading) for target (A,D), bycatch (B,E), and secondary (C,F) vary across a range of target ($\text{esc}_{\text{target}}$) and bycatch ($\text{esc}_{\text{bycatch}}$) minimum escapement levels (i.e., minimum biomass allowed to escape the fishery used in policy, see Methods). Extinction probabilities are calculated as the fraction of simulations resulting in their extinction after 5 years of fishing across all 400 food webs. The color bars showing extinction rates differ by subplot with the marker "$*$" representing the value obtained in open access. Plots were produced by running model simulations for each food web with values [0.15, 0.3, 0.45, 0.6] for each target and bycatch escapement levels (and all their combinations) and then using spline interpolation to fill the extinction values across a broader continuous range of $\text{esc}_{\text{target}} \in [0.15, 0.6]$ and $\text{esc}_{\text{bycatch}} \in [0, 0.6]$.

bycatch ($\text{esc}_{\text{bycatch}}$). As the minimum escapement level for the target quota is raised above around 0.3, the probabilities of all extinctions begin to fall. Adding a bycatch policy ($\text{esc}_{\text{bycatch}} > 0$) has a limited impact on target species (Fig. 3.3A, D), but it effectively reduces bycatch (Fig. 3.3B, E) and secondary (Fig. 3.3C, F) extinctions once the minimum escapement level of bycatch increases above around 0.10. Interestingly, high minimum escapement levels for both target and bycatch has a similar effect in reducing target and secondary extinctions as a high minimum escapement level for target alone. Further, setting medium-low target and bycatch minimum escapement levels has similar effect on reducing bycatch and secondary extinctions as that of setting a medium-high target

escapement level alone. For example, Fig. 3.3E shows that the probability of bycatch extinctions at target and bycatch escapement levels of 0.25 and 0.15, respectively, is similar to the one achieved by setting a target escapement level of 0.45. Overall, simulations in which the bycatch species is chosen as the species with the lowest biomass in the food web before fishing starts (i.e., the most vulnerable species), exhibit higher extinctions than those where the bycatch species was chosen randomly.

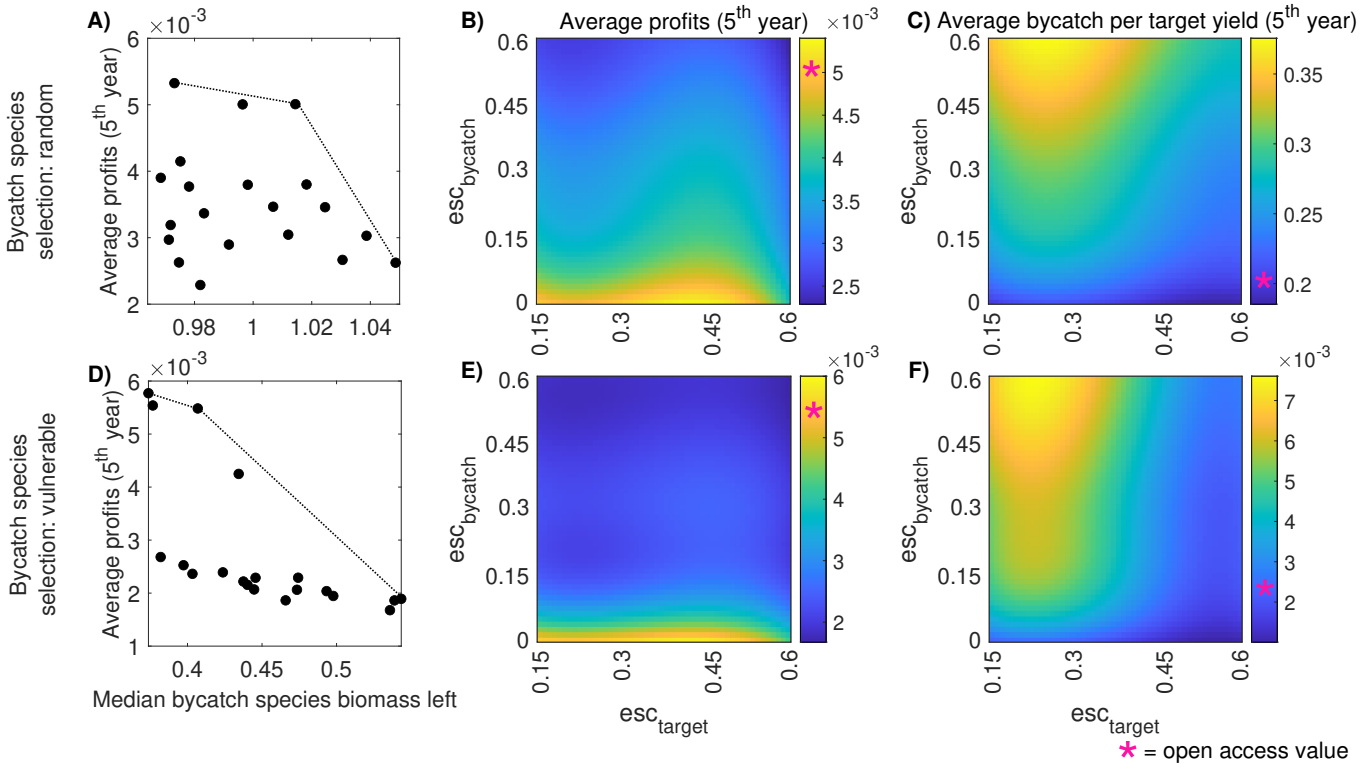

FIGURE 3.4. Economic results for two alternative scenarios of selecting the bycatch species: randomly (A-C) and the most vulnerable species (i.e., species with the lowest biomass, D-F). Average profit (A) and median remaining biomass of the bycatch species (D) were calculated across the 5 fishers and 400 food webs, with all possible target-bycatch combination considered within each food web. Each point corresponds to a given level set for $\text{esc}_{\text{target}}$ and $\text{esc}_{\text{bycatch}}$. The dashed lines trace out the frontier determining the maximum profit for a given unit of bycatch-species' biomass left (or alternatively the maximum bycatch-species' biomass achievable for a given profit). The color bars showing extinction rates differ by subplot with the marker "$*$" representing the value obtained in open access. All results are for the final (fifth) year of fishing to mitigate transient effects apparent in early periods when fishing is first initiated.

We then analyze the economic results of our model in year 5, to exclude transient dynamics in the first four years stemming from the initiation of fishing. We calculated average profits as:

$$\frac{1}{\mathrm{N}}\sum_{k=1}^{N}\frac{1}{365}\sum_{t=1}^{365}E_{k,t}(\gamma_k p q_{\text{target}} B_{\text{target},t} - c_0), \tag{3.7}$$

where $E_{k,t}$ is the effort of k^{th} fisher on day t and $B_{\text{target},t}$ is the biomass of target species at day t. Figure 3.4A and 3.4D shows profits for each combination of policy scenario (given by $\text{esc}_{\text{target}}$ and $\text{esc}_{\text{bycatch}}$) against the median of the fraction of initial unfished bycatch species biomass that survived after 5 years of fishing. We use the median for the bycatch species biomass left given the strong skew of this distribution (across the simulated collection of 400 food webs, with all possible target-bycatch combination considered within each food web). The frontier of these values (dotted line) illustrates the set of feasible best options, where for a given level of bycatch biomass preserved, the expected profits are maximized. Note that we cannot combine the economic and conservation objectives because the bycatch species is not valued in monetary terms here. We found that the typical biomass remaining (median) of the bycatch species is near its unfished biomass (1.0) when the bycatch species is chosen randomly (Fig. 3.4A), but it is typically less than half of its unfished biomass when the most vulnerable species is caught as bycatch (Fig. 3.4B).

Average profits (Fig. 3.4B and 3.4E) are highest when there is no constraint on bycatch ($\text{esc}_{\text{bycatch}} = 0$) and the minimum target escapement level is in a middle range. At such policy combination, the average profits are higher than in open access (the "*" indicator for open access is below the maximum profit level). This profit-maximizing point is associated with some reduction in extinct risks across all species (see Fig. 3.3). Limiting bycatch via a quota reduces extinctions but also expected profits (Fig. 3.4B, E). This tradeoff is stronger when the bycatch species is vulnerable (Fig. 3.4E) rather than randomly chosen (Fig. 3.4B). Finally, we find that the policy zone that minimizes bycatch per unit of target species harvested (top-left corner Fig. 3.4C, F) is different from the zone that minimizes extinctions (top-right corner of all panels in Fig. 3). Further we find that the bycatch per unit of target species can be worse (higher) than that achieved in open access, specifically when there is not constraint on bycatch but the constraint on target species harvest is stringent (high $\text{esc}_{\text{target}}$). More generally, we find that the bycatch species yield per unit target species yield first increases and then decreases with increasing target escapement levels. In

contrast, increasing bycatch escapement levels leads monotonically to more bycatch species yield per unit target species yield.

3.4. Discussion

One of the factors that aids extensive use of single species based management (and its subsequent effectiveness in mitigating collapses of fishery) is the abundance of theoretical work, which forms the basis for effective prediction and management [35]. But there are few theoretical studies which address the dynamic interaction of all species in the marine food web, including impacts from human harvest, while considering policy design. We aim to fill this gap by presenting a novel framework that merges ecological networks and bioeconomic elements to facilitate a quantitative assessment of fishery management policies, furthering an integrative Ecosystem-Based Fisheries Management (EBFM) approach [42, 104]. We extend the Allometric Trophic Network framework in fishery studies by incorporating bycatch species, fisher heterogeneity and annual harvestable quotas for target and bycatch species, which leads to limited fishing periods. We show the effects of target and bycatch quotas on ecological outcomes (species local extinction) – which are relevant especially for vulnerable bycatch species – and economic outcomes (profits and bycatch per unit target yield), which are of primary interest in commercial fishing of the target species.

Having a low minimum escapement level for the target species alone can reduce extinctions in target, bycatch and secondary species. This is consistent with previous analyses [47, 122] showing that the effects of harvesting target species propagate through the ecological network impacting non-target species. While those works focused solely on take of target species, we add realism by including unintentional take of bycatch species as part of fishing. Specifically, our model allows us to quantify how target species and bycatch species harvest policies (given by escapement levels) mitigate species extinctions. Having medium-low target and bycatch escapement levels mitigates bycatch and secondary extinctions similarly to having a medium-high target escapement level alone. Furthermore, having high target and bycatch escapement levels reduce extinctions in target and secondary extinctions similarly to having a very high harvest policy for target escapement (Figure 3.3 A, C, D and F). High escapement levels can lead to smaller fishing opportunities in a fishery, potentially driving out fishers and leading to excessive bycatch in other fisheries, as shown in previous literature [100]. Our model aids in better understanding the benefits of these fishery

policies for reducing species extinctions and could potentially aid with setting escapement levels that align with the goals of specific fisheries. Delving into the economic results, we show that there is a combination of target and bycatch species harvest policies (among all escapement combinations possible) which maximizes average profits, for any given level of bycatch species preserved (Figure 3.4 A and D). For some combinations along this frontier, the average profit incurred is higher than under open access (Figure 3.4 B and E), though this involves a trade-off with the conservation of bycatch and secondary species.

A key benefit of our modeling approach is that it allows for the assessment of a wide range of fishery policy stringencies (on constraining removal of target and bycatch species biomass) based on how they perform across a large set of potential food web configurations. Such configurations are rarely exhaustively characterized in practice. And we are aware of no examples in which the biomass level of each species in an extended food web is regularly assessed to inform fishery management. Such information would be valuable but prohibitively costly to carefully assess on an ongoing basis. Such food webs are also likely to vary over space and time. For the time being, given that managers will not have the luxury of full information about the state of a given food web on a regular basis, there is value in identifying target species and bycatch species harvest policies that achieve objectives in a manner robust to an array of potential food web realities.

There are several avenues for future exploration. While we studied a scenario where a single target and bycatch was harvested, the model's flexibility allows for harvesting of multiple species (target or bycatch), which mimics the functioning of most fisheries around the world. Concepts like the Maximum Economic Yield from single species models are difficult to extend to multiple species [69] effectively. And even when done, such attempts to maximize profits over constraints on multiple species often leads to overexploitation of harvested species [119]. We provide an alternative framework which addresses both those problems. We could constrain fishing on multiple species by setting escapement levels specifically for each of them in our model, leading to newer insights into profit maximization amidst the constraints imposed by multiple species. Lastly, the model's structure can be extended to encompass a broader array of policies, such as setting individual limits on target and bycatch species yield for every fishers (as opposed to a shared annual limit determined by the excess of target and bycatch biomasses above escapement levels as implemented in our study) and or penalties when fishers exceed their individual quota [66,114]. Or more complex

fisher efforts, which might dynamically grow or shrink in response to the profits incurred from the fisheries [34]. Our model paves the way for including the complex interactions of different species in the marine food web and their interactions with fishers and policy makers in multi-species fishery, thus furthering our insights into achieving sustainable fisheries.

Code availability

All codes and data used for this project can be found here - https://doi.org/10.5281/zenodo.10891492.

Funding

This work was funded by the US National Science Foundation (NSF), award number DEB-2224915 from the Division of Environmental Biology (DEB).

Acknowledgements

We thank Kayla R. S. Hale for her valuable inputs regarding the Allometric Trophic Network (ATN) framework.

Conclusion

Allow me to introduce you to my dissertation.

APPENDIX A

Supplementary to Chapter 1 and 2

Supplementary Information

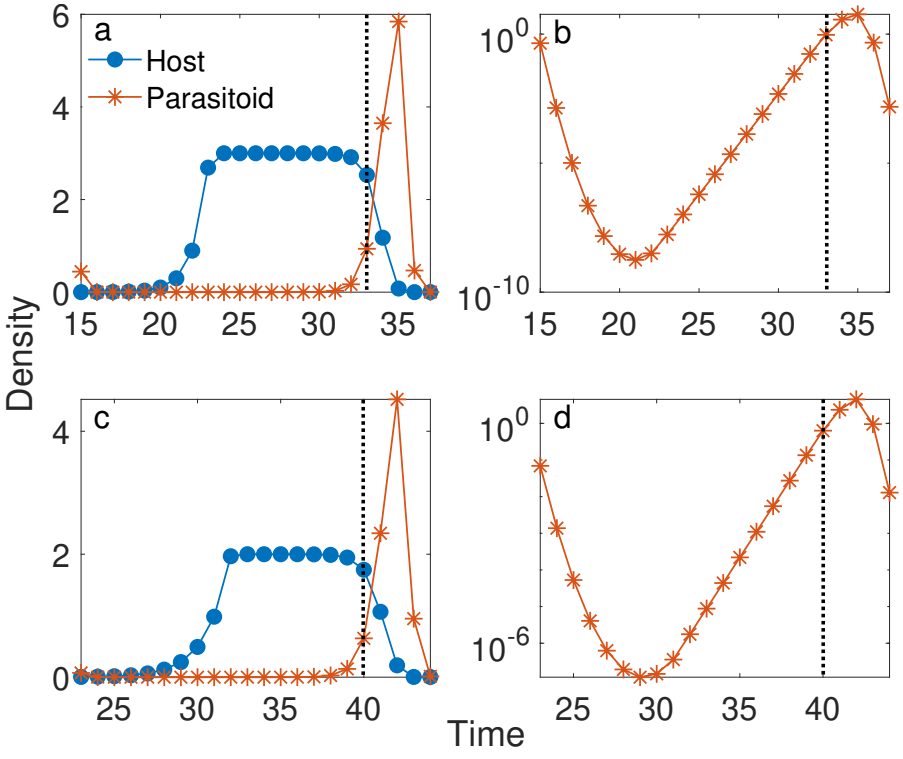

FIGURE A.1. The time series of densities of a host-parasitoid system (in a given cycle) is shown in a) and c) for two different growth parameters. Parasitoid densities are shown in log scale in b) and d), to emphasize the low parasitoid densities attained in each cycle, which is not clear when plotted in linear scale as shown in a) and c). The last generation of outbreak is marked by a dotted vertical line. As shown in b) and d), $p_t \approx 0$ for all of buildup and up until the last generation of outbreak, which is further explained mathematically in [121]. For a) $\lambda = 3$, $\gamma = 6$ and for b) $\lambda = 2$, $\gamma = 5$.

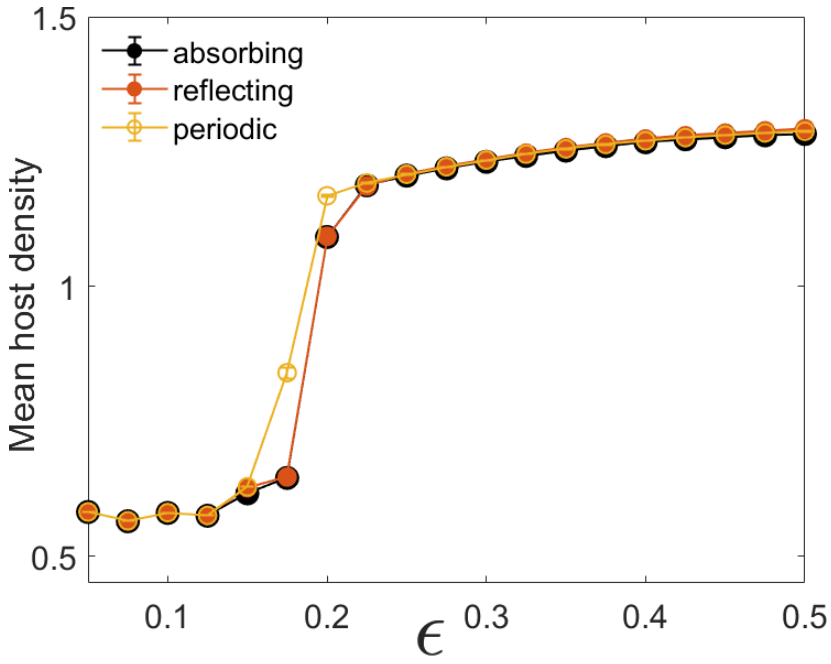

FIGURE A.2. Mean steady-state host densities as a function of migration fraction (ϵ) for absorbing (black), reflecting (orange), and periodic (yellow) boundary conditions in a homogeneous landscape ($\eta = 0$). Error bars represent 95% confidence intervals obtained through bootstrap resampling and are often smaller than the markers. The minimal differences between boundary conditions indicate that, in the absence of heterogeneity, boundary effects are negligible at this system size, where the each side L of our square lattice is $L = 128$. This supports the conclusion that our landscape is sufficiently large for boundary structure to have little impact on overall mean host densities.

Bibliography

[1] K. C. Abbott, *A dispersal-induced paradox: synchrony and stability in stochastic metapopulations*, Ecology Letters, 14 (2011), pp. 1158–1169.

[2] K. C. Abbott and G. Dwyer, *Food limitation and insect outbreaks: complex dynamics in plant-herbivore models*, Journal of Animal Ecology, (2007), pp. 1004–1014.

[3] ——, *Using mechanistic models to understand synchrony in forest insect populations: the north american gypsy moth as a case study*, The American Naturalist, 172 (2008), pp. 613–624.

[4] F. R. Adler, *Migration alone can produce persistence of host-parasitoid models*, The American Naturalist, 141 (1993), pp. 642–650.

[5] D. L. Alverson, *A global assessment of fisheries bycatch and discards*, vol. 339, Food & Agriculture Org., 1994.

[6] C. M. Anderson, M. J. Krigbaum, M. C. Arostegui, M. L. Feddern, J. Z. Koehn, P. T. Kuriyama, C. Morrisett, C. I. Allen Akselrud, M. J. Davis, C. Fiamengo, et al., *How commercial fishing effort is managed*, Fish and Fisheries, 20 (2019), pp. 268–285.

[7] J. L. Anderson, F. Asche, and S. Tveterås, *World fish markets*, Handbook of marine fisheries conservation and management, (2010), pp. 113–123.

[8] R. Arlinghaus, S. J. Cooke, S. Sutton, A. Danylchuk, W. Potts, K. d. M. Freire, J. Alós, E. Da Silva, I. G. Cowx, and R. Van Anrooy, *Recommendations for the future of recreational fisheries to prepare the social-ecological system to cope with change*, Fisheries Management and Ecology, 23 (2016), pp. 177–186.

[9] R. I. Arthur, D. J. Skerritt, A. Schuhbauer, N. Ebrahim, R. M. Friend, and U. R. Sumaila, *Small-scale fisheries and local food systems: Transformations, threats and opportunities*, Fish and Fisheries, 23 (2022), pp. 109–124.

[10] F. Asche and M. D. Smith, *Trade and fisheries: Key issues for the world trade organization*, tech. rep., WTO Staff Working Paper, 2010.

[11] A. Balla, A. Silini, H. Cherif-Silini, A. Chenari Bouket, W. K. Moser, J. A. Nowakowska, T. Oszako, F. Benia, and L. Belbahri, *The threat of pests and pathogens and the potential for biological control in forest ecosystems*, Forests, 12 (2021), p. 1579.

[12] A. J. Barnett and J. M. Anderies, *Weak feedbacks, governance mismatches, and the robustness of social-ecological systems: an analysis of the southwest nova scotia lobster fishery with comparison to maine*, Ecology and Society, 19 (2014).

[13] F. Bastardie, E. J. Brown, E. Andonegi, R. Arthur, E. Beukhof, J. Depestele, R. Döring, O. R. Eigaard, I. García-Barón, M. Llope, et al., *A review characterizing 25 ecosystem challenges to be addressed by an ecosystem approach to fisheries management in europe*, Frontiers in Marine Science, 7 (2021), p. 629186.

[14] J. R. Beddington, D. J. Agnew, and C. W. Clark, *Current problems in the management of marine fisheries*, science, 316 (2007), pp. 1713–1716.

[15] M. Bellanger, C. Macher, M. Merzéréaud, O. Guyader, and C. Le Grand, *Investigating trade-offs in alternative catch share systems: an individual-based bio-economic model applied to the bay of biscay sole fishery*, Canadian Journal of Fisheries and Aquatic Sciences, 75 (2018), pp. 1663–1679.

[16] C. Bellmann, A. Tipping, and U. R. Sumaila, *Global trade in fish and fishery products: An overview*, Marine Policy, 69 (2016), pp. 181–188.

[17] E. L. Berlow, J. A. Dunne, N. D. Martinez, P. B. Stark, R. J. Williams, and U. Brose, *Simple prediction of interaction strengths in complex food webs*, Proceedings of the National Academy of Sciences, 106 (2009), pp. 187–191.

[18] A. A. Berryman, *What causes population cycles of forest lepidoptera?*, Trends in Ecology & Evolution, 11 (1996), pp. 28–32.

[19] O. N. Bjørnstad, R. A. Ims, and X. Lambin, *Spatial population dynamics: analyzing patterns and processes of population synchrony*, Trends in Ecology & Evolution, 14 (1999), pp. 427–432.

[20] A. Boit, N. D. Martinez, R. J. Williams, and U. Gaedke, *Mechanistic theory and modelling of complex food-web dynamics in lake constance*, Ecology letters, 15 (2012), pp. 594–602.

[21] J. R. Boyce, *An economic analysis of the fisheries bycatch problem*, Journal of Environmental Economics and Management, 31 (1996), pp. 314–336.

[22] I. L. Boyd, P. Freer-Smith, C. A. Gilligan, and H. C. J. Godfray, *The consequence of tree pests and diseases for ecosystem services*, Science, 342 (2013), p. 1235773.

[23] D. T. Briese et al., *Classical biological control*, Australian weed management systems, (2000), pp. 161–192.

[24] C. J. Briggs and M. F. Hoopes, *Stabilizing effects in spatial parasitoid–host and predator–prey models: a review*, Theoretical population biology, 65 (2004), pp. 299–315.

[25] J. Brodziak and J. Link, *Ecosystem-based fishery management: what is it and how can we do it?*, Bulletin of Marine Science, 70 (2002), pp. 589–611.

[26] U. Brose, R. J. Williams, and N. D. Martinez, *Allometric scaling enhances stability in complex food webs*, Ecology letters, 9 (2006), pp. 1228–1236.

[27] J. H. Brown, J. F. Gillooly, A. P. Allen, V. M. Savage, and G. B. West, *Toward a metabolic theory of ecology*, Ecology, 85 (2004), pp. 1771–1789.

[28] M. G. Burgess, H. C. Giacomini, C. S. Szuwalski, C. Costello, and S. D. Gaines, *Describing ecosystem contexts with single-species models: a theoretical synthesis for fisheries*, Fish and Fisheries, 18 (2017), pp. 264–284.

[29] L. Caltagirone, *Landmark examples in classical biological control*, Annual Review of Entomology, 26 (1981), pp. 213–232.

[30] C. Chaboud and P. Vendeville, *Evaluation of selectivity and bycatch mitigation measures using bioeconomic modelling. the cases of madagascar and french guiana shrimp fisheries*, Aquatic living resources, 24 (2011), pp. 137–148.

[31] D. Chagaris, M. Allen, and E. Camp, *Modeling temporal closures in a multispecies recreational fishery reveals tradeoffs associated with species seasonality and angler effort dynamics*, Fisheries Research, 210 (2019), pp. 106–120.

[32] P. J. Cohen, J. E. Cinner, and S. Foale, *Fishing dynamics associated with periodically harvested marine closures*, Global Environmental Change, 23 (2013), pp. 1702–1713.

[33] H. Comins, M. Hassell, and R. May, *The spatial dynamics of host–parasitoid systems*, Journal of Animal Ecology, (1992), pp. 735–748.

[34] J. M. Conrad, *Resource economics*, Cambridge University Press, 1999.

[35] J. M. Conrad and D. Rondeau, *Natural resource economics: analysis, theory, and applications*, Cambridge University Press, 2020.

[36] A. Curtsdotter, A. Binzer, U. Brose, F. de Castro, B. Ebenman, A. Eklöf, J. O. Riede, A. Thierry, and B. C. Rall, *Robustness to secondary extinctions: comparing trait-based sequential deletions in static and dynamic food webs*, Basic and Applied Ecology, 12 (2011), pp. 571–580.

[37] P. M. Cury, *Tuning the ecoscope for the ecosystem approach to fisheries*, Marine Ecology Progress Series, 274 (2004), pp. 272–275.

[38] C. L. Delgado, *Fish to 2020: Supply and demand in changing global markets*, vol. 62, WorldFish, 2003.

[39] Á. Einarsson and Á. D. Óladóttir, *Fisheries and Aquaculture: The Food Security of the Future*, Academic Press, 2020.

[40] L. Fahrig, *Effects of habitat fragmentation on biodiversity*, Annual review of ecology, evolution, and systematics, 34 (2003), pp. 487–515.

[41] FAO, *Fisheries management 2: The ecosystem approach to fisheries*, FAO Technical Guidelines for Responsible Fisheries, (2003).

[42] M. J. Fogarty, *The art of ecosystem-based fishery management*, Canadian Journal of Fisheries and Aquatic Sciences, 71 (2014), pp. 479–490.

[43] R. Fujita, *The assessment and management of data limited fisheries: Future directions*, Marine Policy, 133 (2021), p. 104730.

[44] K. J. Gandhi and D. A. Herms, *Direct and indirect effects of alien insect herbivores on ecological processes and interactions in forests of eastern north america*, Biological Invasions, 12 (2010), pp. 389–405.

[45] B. Gauzens, B. C. Rall, V. Mendonça, C. Vinagre, and U. Brose, *Biodiversity of intertidal food webs in response to warming across latitudes*, Nature Climate Change, 10 (2020), pp. 264–269.

[46] J. F. Gillooly, J. H. Brown, G. B. West, V. M. Savage, and E. L. Charnov, *Effects of size and temperature on metabolic rate*, science, 293 (2001), pp. 2248–2251.

[47] P. Glaum, V. Cocco, and F. S. Valdovinos, *Integrating economic dynamics into ecological networks: The case of fishery sustainability*, Science advances, 6 (2020), p. eaaz4891.

[48] H. C. Godfray, M. P. Hassell, and R. D. Holt, *The population dynamic consequences of phenological asynchrony between parasitoids and their hosts*, Journal of Animal Ecology, (1994), pp. 1–10.

[49] E. E. Goldwyn and A. Hastings, *When can dispersal synchronize populations?*, Theoretical population biology, 73 (2008), pp. 395–402.

[50] B. T. Grenfell, O. N. Bjørnstad, and J. Kappey, *Travelling waves and spatial hierarchies in measles epidemics*, Nature, 414 (2001), pp. 716–723.

[51] M. Gyllenberg, G. Söderbacka, and S. Ericsson, *Does migration stabilize local population dynamics? analysis of a discrete metapopulation model*, Mathematical Biosciences, 118 (1993), pp. 25–49.

[52] K. R. Hale, F. S. Valdovinos, and N. D. Martinez, *Mutualism increases diversity, stability, and function of multiplex networks that integrate pollinators into food webs*, Nature Communications, 11 (2020), p. 2182.

[53] S. J. Hall, R. Hilborn, N. L. Andrew, and E. H. Allison, *Innovations in capture fisheries are an imperative for nutrition security in the developing world*, Proceedings of the National Academy of Sciences, 110 (2013), pp. 8393–8398.

[54] S. J. Hall and B. Mainprize, *Towards ecosystem-based fisheries management*, Fish and Fisheries, 5 (2004), pp. 1–20.

[55] I. Hanski, *Metapopulation ecology*, Oxford University Press, 1999.

[56] M. Hassell, *Host–parasitoid population dynamics*, Journal of Animal Ecology, 69 (2000), pp. 543–566.

[57] M. Hassell and J. Waage, *Host-parasitoid population interactions*, Annual review of entomology, 29 (1984), pp. 89–114.

[58] M. P. Hassell, H. N. Comins, and R. M. Mayt, *Spatial structure and chaos in insect population dynamics*, Nature, 353 (1991), pp. 255–258.

[59] A. Hastings, *Complex interactions between dispersal and dynamics: lessons from coupled logistic equations*, Ecology, 74 (1993), pp. 1362–1372.

[60] ——, *Transient dynamics and persistence of ecological systems*, Ecology Letters, 4 (2001), pp. 215–220.

[61] A. Hastings and S. Harrison, *Metapopulation dynamics and genetics*, Annual review of Ecology and Systematics, (1994), pp. 167–188.

[62] A. C. Haynie, R. L. Hicks, and K. E. Schnier, *Common property, information, and cooperation: commercial fishing in the bering sea*, Ecological Economics, 69 (2009), pp. 406–413.

[63] R. Hilborn, *Future directions in ecosystem based fisheries management: a personal perspective*, Fisheries Research, 108 (2011), pp. 235–239.

[64] R. Hilborn, R. O. Amoroso, C. M. Anderson, J. K. Baum, T. A. Branch, C. Costello, C. L. De Moor, A. Faraj, D. Hively, O. P. Jensen, et al., *Effective fisheries management instrumental in improving fish stock status*, Proceedings of the National Academy of Sciences, 117 (2020), pp. 2218–2224.

[65] R. Hilborn and D. Ovando, *Reflections on the success of traditional fisheries management*, ICES journal of Marine Science, 71 (2014), pp. 1040–1046.

[66] D. S. Holland, *Collective rights–based fishery management: a path to ecosystem-based fishery management*, Annual Review of Resource Economics, 10 (2018), pp. 469–485.

[67] R. D. Holt, *Population dynamics in two-patch environments: some anomalous consequences of an optimal habitat distribution*, Theoretical population biology, 28 (1985), pp. 181–208.

[68] R. D. Holt and M. Barfield, *Trophic interactions and range limits: the diverse roles of predation*, Proceedings of the Royal Society B: Biological Sciences, 276 (2009), pp. 1435–1442.

[69] E. Hoshino, S. Pascoe, T. Hutton, T. Kompas, and S. Yamazaki, *Estimating maximum economic yield in multispecies fisheries: a review*, Reviews in Fish Biology and Fisheries, 28 (2018), pp. 261–276.

[70] D. Howell, A. M. Schueller, J. W. Bentley, A. Buchheister, D. Chagaris, M. Cieri, K. Drew, M. G. Lundy, D. Pedreschi, D. G. Reid, et al., *Combining ecosystem and single-species modeling to provide ecosystem-based fisheries management advice within current management systems*, Frontiers in Marine Science, 7 (2021), p. 607831.

[71] C.-h. Hsieh, C. S. Reiss, J. R. Hunter, J. R. Beddington, R. M. May, and G. Sugihara, *Fishing elevates variability in the abundance of exploited species*, Nature, 443 (2006), pp. 859–862.

[72] J. S. Hughes, C. A. Cobbold, K. Haynes, and G. Dwyer, *Effects of forest spatial structure on insect outbreaks: insights from a host-parasitoid model*, The American Naturalist, 185 (2015), pp. E130–E152.

[73] A. F. Hunter and G. Dwyer, *Outbreaks and interacting factors: insect population explosions synthesized and dissected*, Integrative Biology: Issues, News, and Reviews: Published in Association with The Society for Integrative and Comparative Biology, 1 (1998), pp. 166–177.

[74] A. R. Ives, *Continuous-time models of host-parasitoid interactions*, The American Naturalist, 140 (1992), pp. 1–29.

[75] V. A. Jansen, *The dynamics of two diffusively coupled predator–prey populations*, Theoretical Population Biology, 59 (2001), pp. 119–131.

[76] C. Jorgensen, K. Enberg, E. Dunlop, R. Arlinghaus, D. Boukal, K. Brander, B. Ernande, A. Gardmark, F. Johnston, S. Matsumura, et al., *The role of fisheries-induced evolution-response*, Science, 320 (2008), pp. 48–50.

[77] V. Kahui, *A bioeconomic model for hooker's sea lion bycatch in new zealand*, Australian journal of agricultural and resource economics, 56 (2012), pp. 22–41.

[78] N. Kamata and A. Liebhold, *Are population cycles and spatial synchrony a universal characteristic of forest insect populations?*, Population Ecology, 42 (2000).

[79] N. J. Kath, A. Boit, C. Guill, and U. Gaedke, *Accounting for activity respiration results in realistic trophic transfer efficiencies in allometric trophic network (atn) models*, Theoretical Ecology, 11 (2018), pp. 453–463.

[80] M. J. Keeling, O. N. Bjørnstad, and B. T. Grenfell, *Metapopulation dynamics of infectious diseases*, in Ecology, genetics and evolution of metapopulations, Elsevier, 2004, pp. 415–445.

[81] A. Kuparinen, A. Boit, F. S. Valdovinos, H. Lassaux, and N. D. Martinez, *Fishing-induced life-history changes degrade and destabilize harvested ecosystems*, Scientific reports, 6 (2016), p. 22245.

[82] A. Kushal and A. Hastings, *Effect of migrations on synchrony in host-parasitoid system*, Journal of Theoretical Biology, 590 (2024), p. 111855.

[83] M. A. Leibold, M. Holyoak, N. Mouquet, P. Amarasekare, J. M. Chase, M. F. Hoopes, R. D. Holt, J. B. Shurin, R. Law, D. Tilman, et al., *The metacommunity concept: a framework for multi-scale community ecology*, Ecology letters, 7 (2004), pp. 601–613.

[84] S. A. Levin, *Dispersion and population interactions*, The American Naturalist, 108 (1974), pp. 207–228.

[85] S. A. Levin, *The problem of pattern and scale in ecology: The robert h. macarthur award lecture*, Ecology, 73 (1992), pp. 1943–1967.

[86] A. Liebhold and B. Bentz, *Insect disturbance and climate change*, US Department of Agriculture, Forest Service, Climate Change Resource Center. www. fs. usda. gov/ccrc/topics/insectdisturbance/insect-disturbance, (2011).

[87] A. Liebhold, W. D. Koenig, and O. N. Bjørnstad, *Spatial synchrony in population dynamics*, Annu. Rev. Ecol. Evol. Syst., 35 (2004), pp. 467–490.

[88] J. S. Link, *What does ecosystem-based fisheries management mean*, Fisheries, 27 (2002), pp. 18–21.

[89] J. S. Link and A. R. Marshak, *Characterizing and comparing marine fisheries ecosystems in the united states: determinants of success in moving toward ecosystem-based fisheries management*, Reviews in Fish Biology and Fisheries, 29 (2019), pp. 23–70.

[90] R. J. Marasco, D. Goodman, C. B. Grimes, P. W. Lawson, A. E. Punt, and T. J. Quinn II, *Ecosystem-based fisheries management: some practical suggestions*, Canadian Journal of Fisheries and Aquatic Sciences, 64 (2007), pp. 928–939.

[91] N. Martinez, P. Tonnin, B. Bauer, R. Rael, R. Singh, S. Yoon, I. Yoon, and J. Dunne, *Sustaining economic exploitation of complex ecosystems in computational models of coupled human-natural networks*, in Proceedings of the AAAI Conference on Artificial Intelligence, vol. 26, 2012, pp. 326–334.

[92] R. May, M. Hassell, R. Anderson, and D. Tonkyn, *Density dependence in host-parasitoid models*, The Journal of Animal Ecology, (1981), pp. 855–865.

[93] R. M. May, *Host-parasitoid systems in patchy environments: a phenomenological model*, The Journal of Animal Ecology, (1978), pp. 833–844.

[94] N. J. Mills and W. M. Getz, *Modelling the biological control of insect pests: a review of host-parasitoid models*, Ecological modelling, 92 (1996), pp. 121–143.

[95] W. W. Murdoch, C. J. Briggs, R. M. Nisbet, W. S. Gurney, and A. Stewart-Oaten, *Aggregation and stability in metapopulation models*, The American Naturalist, 140 (1992), pp. 41–58.

[96] G. NACHMAN, *An acarine predator-prey metapopulation system inhabiting greenhouse cucumbers*, Biological Journal of the Linnean Society, 42 (1991), pp. 285–303.

[97] M. G. Neubert and H. Caswell, *Demography and dispersal: calculation and sensitivity analysis of invasion speed for structured populations*, Ecology, 81 (2000), pp. 1613–1628.

[98] V. M. Nguyen, N. Young, M. Corriveau, S. G. Hinch, and S. J. Cooke, *What is "usable" knowledge? perceived barriers for integrating new knowledge into management of an iconic canadian fishery*, Canadian Journal of Fisheries and Aquatic Sciences, 76 (2019), pp. 463–474.

[99] A. J. Nicholson and V. A. Bailey, *The balance of animal populations.—part i.*, in Proceedings of the zoological society of London, vol. 105, Wiley Online Library, 1935, pp. 551–598.

[100] C. E. O'Keefe, S. X. Cadrin, and K. D. Stokesbury, *Evaluating effectiveness of time/area closures, quotas/caps, and fleet communications to reduce fisheries bycatch*, ICES Journal of Marine Science, 71 (2014), pp. 1286–1297.

[101] G. Ortuño Crespo and D. C. Dunn, *A review of the impacts of fisheries on open-ocean ecosystems*, ICES Journal of Marine Science, 74 (2017), pp. 2283–2297.

[102] O. Ovaskainen, K. Sato, J. Bascompte, and I. Hanski, *Metapopulation models for extinction threshold in spatially correlated landscapes*, Journal of theoretical Biology, 215 (2002), pp. 95–108.

[103] D. Pauly, V. Christensen, and C. Walters, *Ecopath, ecosim, and ecospace as tools for evaluating ecosystem impact of fisheries*, ICES journal of Marine Science, 57 (2000), pp. 697–706.

[104] E. K. Pikitch, C. Santora, E. A. Babcock, A. Bakun, R. Bonfil, D. O. Conover, P. Dayton, P. Doukakis, D. Fluharty, B. Heneman, et al., *Ecosystem-based fishery management*, 2004.

[105] É. E. Plagányi and D. S. Butterworth, *A critical look at the potential of ecopath with ecosim to assist in practical fisheries management*, African Journal of Marine Science, 26 (2004), pp. 261–287.

[106] J. G. Pope, D. S. Macdonald, N. Daan, J. D. Reynolds, and S. Jennings, *Gauging the impact of fishing mortality on non-target species*, ICES Journal of Marine Science, 57 (2000), pp. 689–696.

[107] P. Rohani and G. D. Ruxton, *Dispersal-induced instabilities in host–parasitoid metapopulations*, Theoretical population biology, 55 (1999), pp. 23–36.

[108] K. L. Ryall and L. Fahrig, *Response of predators to loss and fragmentation of prey habitat: a review of theory*, Ecology, 87 (2006), pp. 1086–1093.

[109] F. D. Schneider, U. Brose, B. C. Rall, and C. Guill, *Animal diversity and ecosystem functioning in dynamic food webs*, Nature Communications, 7 (2016), p. 12718.

[110] J. Sherratt, X. Lambin, C. Thomas, and T. Sherratt, *Generation of periodic waves by landscape features in cyclic predator–prey systems*, Proceedings of the Royal Society of London. Series B: Biological Sciences, 269 (2002), pp. 327–334.

[111] J. A. Sherratt, X. Lambin, and T. Sherratt, *The effects of the size and shape of landscape features on the formation of traveling waves in cyclic populations*, The American Naturalist, 162 (2003), pp. 503–513.

[112] B. Skud, *Revised Estimates of Halibut Abundance and the Thompson-Burkenroad Debate*, 1975.

[113] A. D. Smith, C. J. Brown, C. M. Bulman, E. A. Fulton, P. Johnson, I. C. Kaplan, H. Lozano-Montes, S. Mackinson, M. Marzloff, L. J. Shannon, et al., *Impacts of fishing low–trophic level species on marine ecosystems*, Science, 333 (2011), pp. 1147–1150.

[114] D. Squires, J. Kirkley, and C. A. Tisdell, *Individual transferable quotas as a fisheries management tool*, Reviews in Fisheries Science, 3 (1995), pp. 141–169.

[115] M. R. Strand and J. J. Obrycki, *Host specificity of insect parasitoids and predators*, BioScience, 46 (1996), pp. 422–429.

[116] U. R. Sumaila, C. Bellmann, and A. Tipping, *Fishing for the future: An overview of challenges and opportunities*, Marine Policy, 69 (2016), pp. 173–180.

[117] U. R. Sumaila, V. Lam, F. Le Manach, W. Swartz, and D. Pauly, *Global fisheries subsidies: An updated estimate*, Marine Policy, 69 (2016), pp. 189–193.

[118] D. L. Townsend, T. C. Gouhier, and F. Guichard, *Aggregated dispersal reduces spatial synchrony but promotes instability and extinction risk*, Oikos, (2025), p. e11032.

[119] E. Tromeur and L. Doyen, *Optimal harvesting policies threaten biodiversity in mixed fisheries*, Environmental Modeling & Assessment, 24 (2019), pp. 387–403.

[120] P. Turchin, A. Taylor, and J. Reeve, *Dynamical role of predators in population cycles of a forest insect: an experimental test*, Science, 285 (1999), pp. 1068–1071.

[121] J. Umbanhowar and A. Hastings, *The impact of resource limitation and the phenology of parasitoid attack on the duration of insect herbivore outbreaks*, Theoretical Population Biology, 62 (2002), pp. 259–269.

[122] S. Uusi-Heikkilä, T. Perälä, and A. Kuparinen, *Fishing triggers trophic cascade in terms of variation, not abundance, in an allometric trophic network model*, Canadian Journal of Fisheries and Aquatic Sciences, 79 (2022), pp. 947–957.

[123] G. van de Klashorst, J. Les Readshaw, M. W. Sabelis, and R. Lingeman, *A demonstration of asynchronous local cycles in an acarine predator-prey system*, Experimental & applied acarology, 14 (1992), pp. 185–199.

[124] V. Volpert and S. Petrovskii, *Reaction–diffusion waves in biology*, Physics of life reviews, 6 (2009), pp. 267–310.

[125] J. Waage and M. Hassell, *Parasitoids as biological control agents–a fundamental approach*, Parasitology, 84 (1982), pp. 241–268.

[126] E. Wall, F. Guichard, and A. R. Humphries, *Synchronization in ecological systems by weak dispersal coupling with time delay*, Theoretical ecology, 6 (2013), pp. 405–418.

[127] C. J. Walters, V. Christensen, S. J. Martell, and J. F. Kitchell, *Possible ecosystem impacts of applying msy policies from single-species assessment*, ICES Journal of Marine Science, 62 (2005), pp. 558–568.

[128] Z.-Z. Wang, Y.-Q. Liu, S. Min, J.-H. Huang, and X.-X. Chen, *Parasitoid wasps as effective biological control agents*, Journal of Integrative Agriculture, 18 (2019), pp. 705–715.

[129] J. A. Wiens, *Metapopulation dynamics and landscape ecology*, in Metapopulation biology, Elsevier, 1997, pp. 43–62.

[130] R. J. Williams, *Effects of network and dynamical model structure on species persistence in large model food webs*, Theoretical Ecology, 1 (2008), pp. 141–151.

[131] R. J. Williams and N. D. Martinez, *Simple rules yield complex food webs*, Nature, 404 (2000), pp. 180–183.

[132] ——, *Stabilization of chaotic and non-permanent food-web dynamics*, The European Physical Journal B, 38 (2004), pp. 297–303.

[133] K. A. With, *The landscape ecology of invasive spread*, Conservation Biology, 16 (2002), pp. 1192–1203.

[134] K. A. With and A. W. King, *The use and misuse of neutral landscape models in ecology*, Oikos, (1997), pp. 219–229.

[135] P. Yodzis and S. Innes, *Body size and consumer-resource dynamics*, The American Naturalist, 139 (1992), pp. 1151–1175.

[136] S. Zhou, A. D. Smith, A. E. Punt, A. J. Richardson, M. Gibbs, E. A. Fulton, S. Pascoe, C. Bulman, P. Bayliss, and K. Sainsbury, *Ecosystem-based fisheries management requires a change to the selective fishing philosophy*, Proceedings of the National Academy of Sciences, 107 (2010), pp. 9485–9489.